

# **UNDERSTANDING MAGNETIC FLUX LEAKAGE (MFL) SIGNALS FROM MECHANICAL DAMAGE IN PIPELINES – PHASE I**

## **Final Report**

Contract DTPH56-05-T-0001

Prepared by

L. Clapham, V. Babbar, A. Rubinshteyn, R. Hutanu  
and P. Weyman

Prepared for

United States Department of Transportation  
Pipeline and Hazardous Materials Safety Administration

## Table of Contents

1.	Executive Summary .....	1
2.	Introduction and Overall Project Objective .....	4
3.	Summary of All Previous Work .....	5
3.1	MFL and Stress Effects: Key Features .....	5
3.2	Summary of 2004 GRI-Funded Study: MFL Signals from Circular Dents (Modeled and Experimental) .....	6
4.	Specific Objectives of the Current Year .....	9
5.	Work Plan for the Current Year .....	10
6.	Work Performed During the Current Year .....	11
6.1	Experimental Equipment, Samples and Procedures .....	11
6.1.1	MFL Signal Measurement Equipment.....	11
6.1.2	Samples and Denting Apparatus.....	13
6.1.3	Experimental Procedures .....	14
6.2	Experimental MFL Results from Elongated Dents.....	15
6.2.1	MFL <sub>radial</sub> Results: 2:1 Elongated Dents - Underside Scans.....	18
6.2.2	MFL <sub>axial</sub> Results: 2:1 Elongated Dents, Underside Scans.....	21
6.2.3	MFL <sub>circ</sub> Results: 2:1 Elongated Dents, Underside Scans .....	25
6.2.4	Comparison of All Experimental Results, MFL <sub>radial</sub> , MFL <sub>axial</sub> , MFL <sub>circ</sub> ...	28
6.3	Structural FEA Modeling Results.....	29
6.4	Magnetic FEA Modeling and Residual Stress Incorporation Using Magnetic Anisotropy Variations .....	32
6.5	Magnetic FEA Modeling Results: Axially Elongated Dents.....	35
6.5.1	Axially-Elongated Dent: “Background” No Dent, No Stress Case .....	35
6.5.2	Axially-Elongated Dent: Geometry Only Case .....	36
6.5.3	Axially-Elongated Dent: Residual Stress Influences on the MFL <sub>radial</sub> Signal .....	37
6.5.4	Axially-Elongated Dent: Combined Effects of Stress + Geometry .....	40
6.5.5	Axially-Elongated Dent: Comparison of Modeling and Experimental Results.....	43
6.6	Magnetic FEA Modeling Results: Circumferentially Elongated Dents .....	45
6.6.1	Circumferentially-Elongated Dent: Geometry Only Case.....	46
6.6.2	Circumferentially-Elongated Dent: Stress Influences on the MFL <sub>radial</sub> Signal .....	46

6.6.3	Circumferentially-Elongated Dent: Combined Effects of Stress + Geometry.....	47
6.6.4	Circumferentially-Elongated Dent: Comparison of Modeling and Experimental Results .....	48
6.7	Circular Dents with Included Corrosion Pits:-Experimental and Modeling Results.....	49
6.7.1	Experimental Results:-Circular Dent + Corrosion Pit .....	49
6.7.2	Magnetic FEA Modeling Results: Circular Dent + Corrosion Pit.....	54
6.8	Web-Based Database of MFL Signals from Dented Samples .....	57
7.	Conclusions.....	58
8.	References.....	60

## Table of Figures

Figure 1:	Magnetic FEA model used in the 2004 GRI-funded study of MFL signals from circular dents. Only a quarter-model is used because of geometry and loading symmetry considerations. The air box is the rectangular parallelepiped lying between the topmost horizontal surface and lowermost horizontal surface of the model.....	7
Figure 2:	Quarter-model magnetic FEA result for the MFL signal (radial component) shown as a contour plot. This corresponds to the upper right-hand quadrant of the experimental signal shown in Figure 3. ....	8
Figure 3:	Experimental MFL radial component contour plot for a 40-mm diameter circular dent. ....	8
Figure 4:	Schematic diagram of the magnetizer and data acquisition system used to measure MFL signals.....	12
Figure 5:	Tool and die used for creating elongated dents in the present study. Note that the tool and die are completely separate items and in this photo, which shows the tool simply resting on the die.....	13
Figure 6:	Dent created using the elongated denting tool shown in Figure 5. a) topside of dent, b) underside of dent.....	14
Figure 7:	Illustration of hypothetical data collection points along topside of sample....	14
Figure 8:	Illustration of hypothetical data collection points along underside of sample.	14
Figure 9:	The Hall sensor maintains its orientation parallel to the sample in the x-plane. ....	15
Figure 10:	MFL <sub>radial</sub> plots for 40mm diameter circular dents of 3mm and 7mm depths, before and after annealing.....	17
Figure 11:	Preannealed and annealed underside MFL <sub>radial</sub> result for axially-oriented dent.....	19
Figure 12:	Preannealed and annealed underside MFL <sub>radial</sub> result for circumferentially-oriented dent.....	20
Figure 13:	MFL <sub>radial</sub> peak to peak results from the underside of the dent before and after annealing.....	21
Figure 14:	Pre-annealed and annealed underside MFL <sub>axial</sub> result for axially-oriented dent.....	22
Figure 15:	Preannealed and annealed underside MFL <sub>axial</sub> result for circumferentially-oriented dent.....	23
Figure 16:	MFL <sub>axial</sub> peak to peak results – underside, before and after annealing. ....	24
Figure 17:	Preannealed and annealed underside MFL <sub>circ</sub> result for axially-oriented dent. ....	26

Figure 18: Preannealed and annealed underside MFL <sub>circ</sub> result for circumferentially-elongated dents.....	27
Figure 19: MFL <sub>circ</sub> peak to peak results, underside, before and after annealing. ....	28
Figure 20: The modeled tool, die and plate used for obtaining the residual stress patterns for elongated dents in the present study.....	29
Figure 21. Residual normal stress in the x direction for a 2:1 aspect ratio, 4mm deep dent. ....	30
Figure 22. Residual normal stress in the y direction for a 2:1 aspect ratio, 4mm deep dent. ....	30
Figure 23. Residual normal stress in the z (through-wall) direction for a 2:1 aspect ratio, 4 mm deep dent. ....	31
Figure 24. Residual shear stress in the xy plane for a 2:1 aspect ratio, 4mm deep dent. .	31
Figure 25. Quarter model of the elongated dent, used for magnetic finite element modeling. ....	33
Figure 26. Contour map (top) and surface plot (bottom) of the MFL <sub>radial</sub> component for the ‘no dent no stress’ (background) case obtained by magnetic FEA modeling. ....	35
Figure 27. Comparison of modeled and experimental results for the “geometry only” evaluation of the 5-mm deep axially-oriented dent. ....	36
Figure 28. Assignment of H <sub>k</sub> values for normal y stresses.....	37
Figure 29. Assignment of H <sub>k</sub> values for shear stresses.....	37
Figure 30. The contributions of normal residual circumferential (y) stresses on the MFL <sub>radial</sub> signal.....	38
Figure 31. MFL pattern due to all the shear stresses shown in Fig. 29.....	39
Figure 32. Quarter dent segments showing (a) lower half, high y-compressive stress region, (b) lower half, low y-compressive stress region (light blue) adjacent to a higher y-compressive stress region (dark blue), and (c) upper half, low y-tensile stress region (light yellow) adjacent to a high y-tensile stress region (dark yellow). ....	40
Figure 33. Effect on the MFL <sub>radial</sub> signal of all of the ‘straight rim’ circumferential (y) stresses shown in Figure 32. ....	40
Figure 34. Combined effect of the normal circumferential (y) stresses (including straight and curved rim) and shear stresses on the MFL <sub>radial</sub> pattern. ....	41
Figure 35. Geometry-only MFL <sub>radial</sub> pattern shown earlier, reproduced here for ready comparison with Figures 34 and 36. ....	42
Figure 36. Final combined geometry + stress MFL <sub>radial</sub> pattern for the 5-mm deep, axially-elongated 2:1 dent.....	43

Figure 37. Experimental MFL <sub>radial</sub> smoothed contour plot for an axially-elongated 2:1 dent of 5-mm depth (unannealed). .....	44
Figure 38. Experimental MFL <sub>radial</sub> contour plot from a 4:1 axially-oriented dent of a) 5mm depth and b) 6mm depth. ....	45
Figure 39. Comparison of modeled and experimental results for the “geometry only” evaluation of the 5-mm deep circumferentially-oriented dent.....	46
Figure 40. Effect on the MFL <sub>radial</sub> signal of all of relevant stresses in and around the circumferentially-oriented, 2:1 5 mm deep dent.....	47
Figure 41. Final combined geometry + stress MFL <sub>radial</sub> pattern for the 5-mm deep, circumferentially-elongated 2:1 dent. ....	48
Figure 42: Experimental MFL <sub>radial</sub> contour plot for a circumferentially-elongated dent of depth 5 mm (unannealed). ....	49
Figure 43. Underside MFL <sub>radial</sub> plots for (a) a 3mm diameter through-wall corrosion pit in an undented plate, (b) a 3mm diameter blind pit in a 3mm deep circular dent, and (c) a 3mm diameter through-wall pit in a 5mm diameter deep circular dent.....	51
Figure 44. Underside MFL <sub>axial</sub> plots for (a) a 3mm diameter through-wall corrosion pit in an undented plate, (b) a 3mm diameter blind pit in a 3mm deep circular dent, and (c) a 3mm diameter through-wall pit in a 5mm deep circular dent.....	52
Figure 45. Underside MFL <sub>circ</sub> plots for (a) a 3mm diameter through-wall corrosion pit in an undented plate, (b) a 3mm diameter blind pit in a 3mm deep circular dent, and (c) a 3mm diameter through-wall pit in a 5mm circular dent. ....	53
Figure 46. Magnetic FEA MFL <sub>radial</sub> model results for circular dent + corrosion defect. ....	54
Figure 47. Magnetic FEA MFL <sub>axial</sub> model results for circular dent + corrosion defect. ..	55
Figure 48. Underside MFL <sub>radial</sub> component, corrosion pit + circular dent. ....	56
Figure 49. Database of MFL results for dented samples - topside and underside. ....	57

## Table of Tables

Table 1. Magnetic FEA model used in the 2004 GRI-funded study of MFL signals from circular dents.....	15
---	----

## **UNDERSTANDING MAGNETIC FLUX LEAKAGE (MFL) SIGNALS FROM MECHANICAL DAMAGE IN PIPELINES – PHASE I**

### **1. Executive Summary**

Pipeline inspection tools based on Magnetic Flux Leakage (MFL) principles represent the most cost-effective method for in-line detection and monitoring of pipeline corrosion defects. Mechanical damage also produces MFL signals, but as yet these signals are not sufficiently well characterized and understood to be used for reliable mechanical damage detection and characterization. The objective of this project is to accurately model MFL signals produced by mechanical damage in pipelines using finite element structural and magnetic modeling techniques. This report summarizes the findings of the first year (Phase 1) of what is anticipated to be a three year study. Previous work involved preliminary experimental work and modeling studies of circular plain\* dents in plate samples dented using a hydraulic press. In this current year the work was extended to include dents which are elongated in both the axial and circumferential direction, having a 2:1 aspect ratio. Work in future years will extend the study to more realistic dents in pipe sections, as well as gouges and dents+gouges. Ultimately the final, validated magnetic model, along with corresponding experimental measurements, will be used to produce a comprehensive dent/gouge MFL signal library. This can be made accessible to stakeholders (pipeline operators and inspection tool vendors) to assist in accurately interpreting mechanical damage from MFL signals.

The work involves a combination of modeling and experimental studies. On the modeling side, structural finite element analysis (FEA) modeling is used to evaluate the likely stress distribution around a dent. Elastic strain information from these structural FEA models is used to assign values to magnetic permeability functions, which are then incorporated into magnetic FEA models for MFL signal prediction. These magnetic FEA models are used to study the effects of both dent geometry and dent stress on the MFL signals.

Experimental work parallels that of the modeling work. Dents of varying depths (3mm-8mm) are produced in 3mm thick steel plate samples. Full contour plots of MFL signals from these dents are then obtained in each of the radial, axial, and circumferential component directions. Selected dents are stress-relieved using standard annealing treatments, and then re-measured to examine the difference between the 'geometry+strain' and 'geometry-only' strain signals. These experimental signals are then compared to the modeling results in order to verify and further refine the models.

The results of the current year study are summarized below

---

\* 'plain' dents are those in which no gouge is present

### 1. Experimental comparison of $MFL_{\text{radial}}$ , $MFL_{\text{axial}}$ and $MFL_{\text{circ}}$ dent signals

Experimental studies examined both topside and also underside MFL signals from a range of depths, both in the axial and circumferential orientation. The following points were noted:

- The  $MFL_{\text{radial}}$  signal component consistently displays the largest and most detailed signals. This is due to the fact that the sensor lies closer to the surface in this orientation than in the other two.
- The  $MFL_{\text{radial}}$  and  $MFL_{\text{circ}}$  signals contain distinct stress-related and also geometry-related features (peaks). In general the central peaks tend to be geometry related, with dent rim stresses reflected in shoulder peaks. The  $MFL_{\text{axial}}$  component appears to have no specific stress-related features and also appears similar to signals produced by corrosion pits.
- All MFL signal features diminish slightly with stress-relief annealing, however the magnitude of the shoulder peaks is considerably affected by annealing, reinforcing the conclusion that they tend to be related to residual stress.

A major conclusion from this aspect of the work is that, for dent detection and sizing, inspection tools should measure all three components of the MFL signal, rather than just the  $MFL_{\text{axial}}$  signal as is typical in most cases.

### 2. Axially-elongated 2:1 aspect ratio dents: modeling and experimental studies

Both geometry and stress have considerable and interesting effects on the axially elongated dent signals:

- The geometry signal displays a characteristic ‘4 peak’  $MFL_{\text{radial}}$  signature along the line of the dent in the applied field direction. The two outside peaks are associated with the outer dent rim ‘corner’, while the two inner peaks originate from the corner at the dent base. This result is similar to that seen in circular dents – however as the dent aspect ratio increases the peaks migrate further away from the dent centre.
- The main stress contribution to the  $MFL_{\text{radial}}$  signal is associated with the dent rim ‘sidewall’ – i.e. the rim along the long side of the dent. This produces a significant vertical peak which tends to be positioned approximately over the central dent geometry peak.
- The combined effect of stress+geometry on  $MFL_{\text{radial}}$  signals is very interesting in this case, since the dent sidewall stress contribution lies over the inner dent geometry peak but is of opposite polarity. This has two effects –
  1. to diminish the size of the inner geometry peak
  2. to ‘create’ an apparent additional peak in the centre dent sidewall rim region. This peak is actually a composite of geometry+stress effects.

This is particularly notable because accurate interpretation of this signal would likely have been impossible without the contribution from the modeling study.

### 3. Circumferentially-elongated 2:1 aspect ratio dents: modeling and experimental studies

The results of experimental and modeling studies for the  $MFL_{\text{radial}}$  signals for circumferentially-oriented elongated dents are summarized below:



- The geometry signal comprise 4 peaks as with the earlier circular and axial dent cases, however due to the circumferential elongation of the dent these central peaks are much closer together and also elongated.
- Sidewall dent rim stresses have little effect on the MFL signal in this orientation. The stress effects on the signal are mainly in the form of shoulder peaks at the extreme ends of the signal (in the circumferential direction).
- Combined stress + geometry signals are relatively simple to interpret in this case and represent a straightforward superposition of the two effects on the signal.

#### **4. Circular dents containing corrosion pits: modeling and experimental studies**

This aspect of the current year study was undertaken to examine the combined MFL signals from pits located within circular dents. Through-wall pits of 2, 4 and 24mm were created in 40mm diameter circular dents. Both modeling and experimental work indicated that the MFL signals for the combined pit+dent were a simple superposition of the two signals. The pit was centered in the middle of the dent, so clear signals from pit and dent were seen when the dent was relatively small. In the 24mm diameter pit there was considerable overlap with signals and interpretation became more difficult.

#### **5. Web-based database – preliminary work**

The ultimate goal of this project is to be able to have MFL signal results from dents of known shapes and stresses. With a very large number of results, effective presentation becomes an issue. We present a relatively simple proposed format for a web-based, results spreadsheet which should allow for easy access to both modeled and experimental results of this study. Further development of this database will proceed as the project evolves.

Overall, our study thus far has proved to be extremely successful – with the magnetic models helping to interpret many details and features of MFL signals that will prove to be extremely important in establishing dent severity. Currently all work is on-time and on-budget, and funding has been secured for the remaining two years of the study from both PRCI and the DOT.

## 2. Introduction and Overall Project Objective

Pipeline inspection tools based on Magnetic Flux Leakage (MFL) principles represent the most cost-effective method for in-line detection and monitoring of pipeline corrosion defects. These tools have been in commercial use for over three decades. Mechanical damage produces MFL signals, but as yet these signals are not sufficiently well characterized and understood to be used for reliable mechanical damage detection and characterization. The objective of this project is to accurately model MFL signals produced by mechanical damage in pipelines using finite element structural and magnetic modeling techniques. The final, validated magnetic model, along with corresponding experimental measurements, will be used to produce a comprehensive dent/gouge MFL signal library made accessible to inspection vendors and pipeline operators for use in interpreting MFL signals from mechanical damage defects.

MFL signals from dents include a geometry component in addition to a component due to residual stresses. The relative contribution of each of these components to the MFL signal depends on the size and shape of the dent in addition to other effects such as metal loss, gouging, corrosion, etc. In this project, magnetic Finite Element Analysis (FEA) is used to model both the residual stress and geometry contributions to the MFL signal. Corresponding experimental studies are used to validate predictions and further refine the model, as well as to examine the effect of dent depth on the MFL signals.

The Applied Magnetics Group (AMG) at Queen's University began working on mechanical damage in 2002. In 2002 and 2003, mechanical damage modeling formed a relatively small part (~30%) of a larger Gas Research Institute (GRI)-funded AMG project (GRI Contracts # 5093-260-2605 and 5093-260-8682) and examining stress effects on MFL signals. At this early stage, the magnetic modeling software\* was limited in its geometric modeling capabilities; i.e., the dent shape could not be accurately modeled. In 2004, an improved version of the software was released with vastly improved geometrical modeling capability. This capability, combined with experience gained through project work for GRI on modeling stress effects on MFL signals enabled construction of magnetic MFL models that accurately represent both the dent geometry and associated stress distribution. GRI funding in 2004 enabled further work on modeling and corresponding experimental efforts on simple circular dents in steel plate samples.

The current 2005/06 study (year-end of March 31, 2006) is the first year of a 3-year project that includes the following tasks:

- Year 1 (April 2005-March 2006): Magnetic modeling of MFL signals from simple dents (without gouges) in steel plate. Elongated dents with a 2:1 aspect ratio and long axis oriented in either the axial or circumferential directions were considered,

---

\* AMG uses Infolytica MagNet magnetic modeling software, which is the only magnetic modeling software that allows for the incorporation of "stresses" into the magnetic model via local modifications of the magnetic permeability functions.

Corresponding experimental work was conducted to verify magnetic models and examine dent depth effects.

- Year 2 (April 2006-March 2007): Extension of Year 1 work on plain dents (dents without gouges) to a modeling and experimental study of backhoe-created dents in pipeline sections. Samples will be produced by Gaz de France in their mechanical-damage laboratory using a device that creates, as realistically as possible, dents that would be caused from pipeline impacts from various heavy equipment.
- Year 3 (April 2007-March 2008): Modeling and experimental work on dents containing gouges. Gaz de France will provide dented+gouged samples for experimental MFL measurements at the AMG laboratory.

### **3. Summary of All Previous Work**

#### **3.1 MFL and Stress Effects: Key Features**

The MFL inspection technique involves applying a direct current (DC), axially-oriented magnetic field to the pipe wall using a set of large permanent magnets. The pipe wall is magnetized to near-saturation. Therefore, in regions of metal loss (such as a corrosion pit), some of the magnetic flux is forced (or ‘leaks’) into the surrounding air. A Hall probe or detector coil mounted between the magnet pole pieces detects this “leaking” flux as an MFL signal.

In corrosion detection, the size of the MFL signal correlates to the size of the corrosion region. However, a complicating factor in corrosion signal interpretation is the influence of stress. This is due to the fact that magnetism is strongly stress dependent, and that there are many different ‘sources’ of stress in an operating pipeline – applied (pressurization) stresses, residual stresses introduced during manufacturing and installation, in addition to stress concentrations around the defects themselves. In what is now recognized as a classic paper in the field<sup>[1]</sup>, David Atherton (the founder of the Applied Magnetics Group at Queen’s University) brought attention to the effects of stress on MFL corrosion signals, illustrating that stress may affect the magnitude of these signals by up to 50%. From 1998-2002, the AMG conducted an extensive GRI-funded study to characterize elastic and plastic deformation effects on MFL signals using both experimental and FEA techniques. This work provided an invaluable database of knowledge in this area, which is summarized in GRI reports<sup>[2]</sup> and many technical papers<sup>[3-7]</sup>.

The understanding of stress effects gained in this earlier GRI-funded study is the foundation of the present MFL mechanical damage study. The following selected results from the earlier work are of particular importance:

- Elastic tensile strain creates an increase, and compressive elastic strain a decrease, in the magnetic permeability\* of a pipeline wall. Therefore local pipe wall elastic

---

\* Magnetic permeability is the proportionality constant between applied field and induced flux density in a material. It is, itself, a function of applied field and the local stress level.

strain such as that associated with dents can enhance or decrease MFL signals depending on their sign, magnitude and orientation with respect to the applied MFL field.

- Earlier work has shown that magnetic properties are highly dependent on elastic strain, but very much less sensitive to strain into the plastic regime. Therefore for a plain (ungouged) dent only the elastic (residual) stress is expected to contribute to the MFL signal. It should be noted that gouges include much higher deformation levels, and that the plastically deformed material associated with gouges is expected to have an associated MFL signal. The effect of gouges will be considered in Year 3 of this project.
- Because most of the effects on MFL signals arise from elastic (residual) strain, these effects can be largely removed in laboratory samples by using standard ‘stress relieving’ heat treatments.
- Working closely with Infolytica MagNet FEA software<sup>[8]</sup>, magnetization functions were developed and implemented within the magnetic modeling software to allow the magnetic permeability to be varied both locally and anisotropically (i.e., in the three orthogonal directions). This enables magnetic modeling of the multi-axial effects of stress on MFL signals.
- Extensive experimental testing of samples under stress and applied field conditions provided the critical magnetization function data needed for FEA modeling of stress effects on MFL signals.

### **3.2 Summary of 2004 GRI-Funded Study: MFL Signals from Circular Dents (Modeled and Experimental)\***

In 2003, improvements in the Infolytica MagNet FEA modeling software<sup>[8]</sup> made it possible to accurately represent dent geometries, and in 2004, this capability was extended to model MFL signals from circular dents (without gouges). Figure 1 shows the magnetic model used in the 2004 study\*. A detailed description of the magnetic MFL modeling process applied is provided in Section 5. The discussion that follows provides only a background to description of the 2004 study.

---

\* A detailed summary of this work can be found in reference 9.

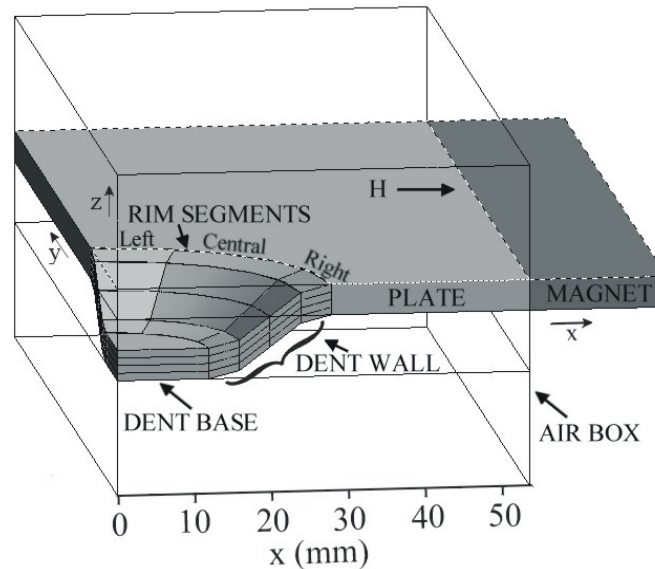


Figure 1: Magnetic FEA model used in the 2004 GRI-funded study of MFL signals from circular dents. Only a quarter-model is used because of geometry and loading symmetry considerations. The air box is the rectangular parallelepiped lying between the topmost horizontal surface and lowermost horizontal surface of the model.

As shown in Figure 1, the circular dent model is divided into ‘dent wall/rim’ and ‘dent base’ regions, and these regions are further subdivided into blocks. Different blocks in a region can be assigned different anisotropic permeability functions, depending on the stress level of those blocks. The stress levels were determined using structural FEA modeling.

The overall FEA-modeled MFL signal (radial component), incorporating both geometry and stress components, is shown in Figure 2. (Note that this is a quarter-model representing the upper right quadrant). Figure 3 shows the experimental MFL (radial component) signal obtained from laboratory measurements on a 40-mm diameter circular dent of 7mm depth. The experimental and modeling results match very closely. Furthermore, since stress effects could readily be turned ‘on’ or ‘off’ in the magnetic FEA model, it was possible to identify the individual effects of stress and dent geometry. These modeling results enabled determination of the origin of each specific feature in the experimental result of Figure 3, specifically:

- The circular dent geometry gives rise to two central peaks (labeled ‘geometry peaks’ in Figure 3) of opposite polarity.
- The stresses in the dent rim create a significant shoulder peak. This appears to combine with the similar polarity outer geometry peak, creating what appears to be a “halo” effect.
- An additional stress peak is also associated with the dent base, but this peak is obscured by the main geometry peak.

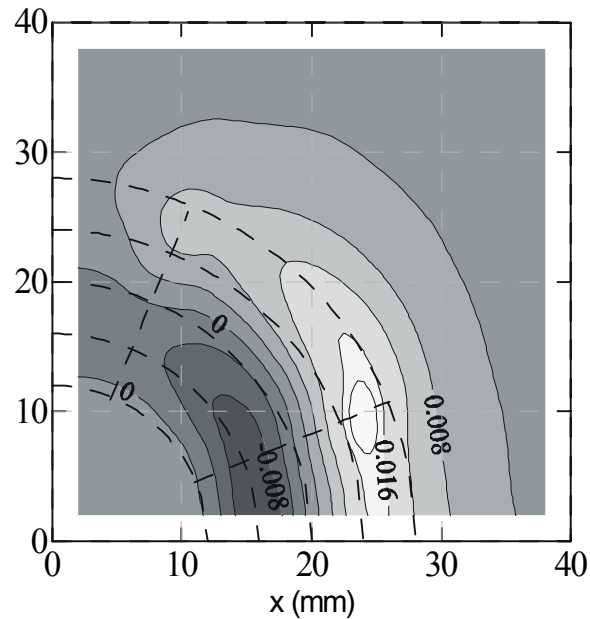


Figure 2: Quarter-model magnetic FEA result for the MFL signal (radial component) shown as a contour plot. This corresponds to the upper right-hand quadrant of the experimental signal shown in Figure 3.

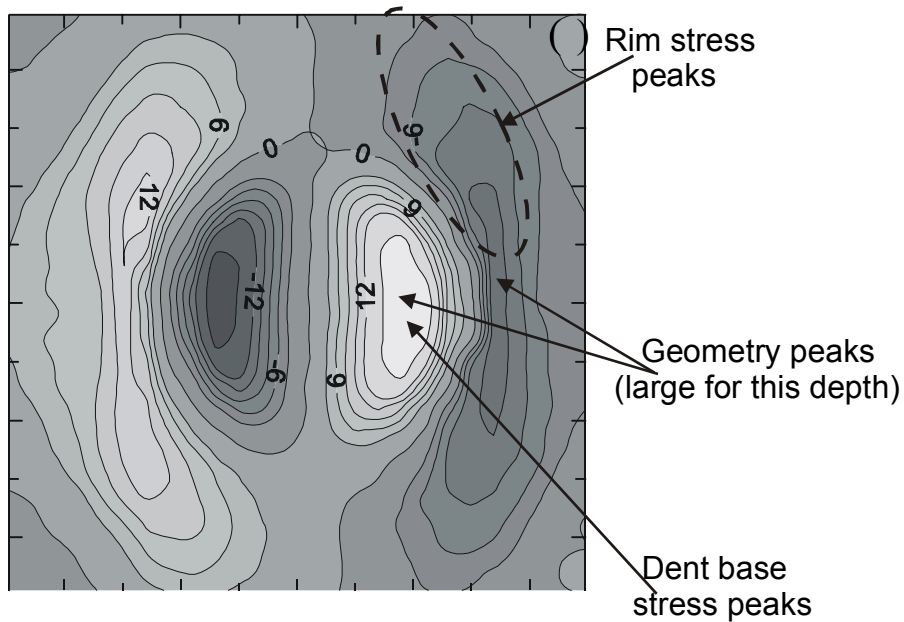


Figure 3. Experimental MFL radial component contour plot for a 40-mm diameter circular dent. The FEA modeled result shown in Figure 2 enabled the individual features of this MFL result to be associated with either geometry of stress as indicated in the diagram. (Note that the peak polarity is reversed compared with Figure 2 because the field is applied in the opposite direction.)

#### **4. Specific Objectives of the Current Year**

As mentioned in Section 2, the 2004 work focused on developing magnetic models that would accurately predict both the stress and geometry-induced components of the MFL signals for simple (no-gouge) circular dents. Experimental work was also conducted to verify and refine the modeling results.

In the current 2005/06 project (ending March 31, 2006) the earlier work was extended to examine elongated dents, and circular dents containing simulated corrosion pits. Specifically, the project objectives were as follows:

- To develop accurate magnetic models for predicting MFL signals from 2:1 aspect ratio dents, elongated in the axial pipe direction (i.e., the direction of the applied magnetic field). Structural FEA modeling was conducted to determine the local stress levels and directions surrounding the dents. Corresponding experimental studies involved obtaining experimental MFL signal measurements from steel plate samples dented to various depths using a 2:1 aspect ratio indentation tool.
- To develop accurate magnetic models for predicting MFL signals from 2:1 aspect ratio dents, elongated in the circumferential pipe direction (i.e., perpendicular to the direction of the applied magnetic field). The structural FEA models applied for the axial case could also be used here since samples were developed from plate rather than pipe material that includes wall curvature. Corresponding experimental studies involved obtaining experimental MFL signal measurements from steel plate samples dented to various depths using a 2:1 aspect ratio indentation tool.
- To develop accurate magnetic models for predicting MFL signals from circular dents containing corrosion pits. Corresponding experimental studies involved obtaining experimental MFL measurements from circular dents containing electrochemically milled corrosion pits.
- To begin developing a web-based MFL signal library database to allow easy access to the MFL dent signals (modeled and experimental) obtained in this study.

## 5. Work Plan for the Current Year

Specific elements of the work plan for the project period starting April 1, 2005 and ending March 31, 2006 are outlined in task list (PHMSA payable milestones table) shown below. Details of the experimental procedures and FEA modeling methods are given in Section 5.

Item Number	Task Number	Payable Milestone Project #90C - MFL	Expected Completion Date (months after award)
1	1.1	Finite element modeling software license renewed	0
2	1.1	Denting tool constructed and tested	3
3	1.2	Modeled stress pattern around oval dents	1
4	1.2	Modeled MFL signals from axially oriented oval dents	3
5	4	First quarterly report submitted	3
6	1.3	Modeled MFL patterns around axially-oriented oval dents	6
7	1.4	Observed experimental MFL patterns around axially-oriented oval dents	6
8	2.1	Modeled stress pattern around dents with corrosion	6
9	4	Second quarterly report submitted	6
10	1.5	Modeled MFL patterns around circumferentially oriented oval dents	9
11	1.6	Observed experimental MFL patterns around circumferentially oriented oval dents	9
12	1.4	Observed Further experimental MFL patterns around axially-oriented oval dents	9
13	2.2	Modeled MFL patterns from circular dents with corrosion pits	9
14	2.3	Observed experimental MFL patterns around circular dents with corrosion pits.	9
15	4	Third quarterly report submitted	9
16	3	Reviewed initial results on MFL from backhoe dents - for use in follow-on magnetic modeling studies.	12
17	4	Final report including database details submitted and conference presentation completed	12



## **6. Work Performed During the Current Year**

An extensive amount of work was performed during the current year, with a considerable amount of data generated. More than 300 experimental MFL contour plots and over 50 magnetic FEA MFL plots were developed. The full listing of experimental results has been included in the Appendices of this report for reference. The individual subsections that follow, which present highlights of the work conducted, provide detail on the following:

- 6.1: Outline of the experimental equipment, techniques and samples
- 6.2: Experimental MFL results from elongated dents (select results)
- 6.3: Structural FEA modeling results used to determine local permeability variations for the magnetic FEA models
- 6.4: Theory and methods for magnetic FEA modeling and stress incorporation
- 6.5: Magnetic FEA modeling results of axially-elongated dents and comparison with selected experimental results
- 6.6: Magnetic FEA modeling results of circumferentially-elongated dents and comparison with selected experimental results
- 6.7: Experimental and modeling results of circular dents with included corrosion pits
- 6.8: Discussion of web-based database

### **6.1 Experimental Equipment, Samples and Procedures**

In the current year the experimental technique applied was similar to that used for previous work on MFL signals from circular dents<sup>[9]</sup>. Earlier work<sup>[12]</sup> showed that residual stress effects (and the associated MFL signals) could be removed using typical stress relieving heat treatments. Therefore, consistent with previous experimental studies, the procedure for experimentally separating stress and geometry components of the MFL signal was as follows:

- Sample denting
- MFL measurements to obtain the overall (stress+geometry) MFL signal
- Stress-relieving heat treatments
- Repeat MFL measurements to obtain the geometry-only MFL signal

#### **6.1.1 MFL Signal Measurement Equipment**

A simple magnetizer circuit was used to measure MFL signals as shown in Figure 4. It consists of NdFeB permanent magnets and backing iron pieces which complete the magnetic circuit and induce the magnetic flux into the sample. The magnetic flux density in the sample can be varied by changing the number of permanent magnets in the magnetic circuit or by varying the cross-sectional area of a backing circuit (not shown). For the purpose of the present study, the background flux density in the samples was maintained at about 1.5T. For comparison, the highest flux densities available in commercial inspection tools are approximately 1.8T, corresponding to magnetic

saturation of the pipe wall. The slightly lower flux density was chosen for the present study because stress effects are more obvious at these lower flux densities.

The presence of a defect diverts some of the flux from the sample into the surrounding air, creating a ‘leaking’ magnetic flux (the MFL signal). This flux is detected using a Hall probe. The Hall probe is scanned in 1mm steps over the entire defect area (typically 50mm x 50 mm) to obtain a full MFL contour or surface plot over the profile of the dent. The main unit of the data acquisition and control system is a personal computer (PC) with a data acquisition board. The system controls the Hall probe scanning system and reads and records the output from the Hall probe amplifier. The Hall probe output is directed into the PC via an amplifier and an analog to digital (A/D) converter.

It is important to note that in the present work the Hall probe was oriented, in separate experiments, to measure each of the radial, axial or circumferential components of the leakage flux. Traditionally, commercial inspection tools have measured only the axial component of the MFL signal, however, many newer tools now have capability to measure all three MFL components. Work within the AMG<sup>[2]</sup> has found that the radial MFL component provides more useful defect information than the other two components. This is particularly important in the present study since the “traditional” axial component MFL signals may not provide the best information for dent signal interpretation.

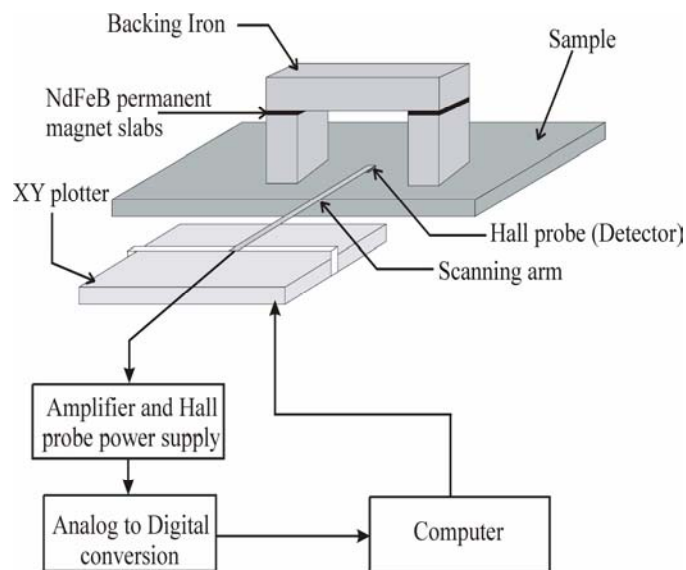


Figure 4. Schematic diagram of the magnetizer and data acquisition system used to measure MFL signals.

### 6.1.2 Samples and Denting Apparatus

Samples of 0.12" (3mm) mild steel thick plate were used in the present study. These are easier to obtain and deform than pipeline samples and earlier work <sup>[2]</sup> indicated mild steel is similar to pipeline steel with respect to magnetic behavior. Prior to denting, the samples were stress relieved at 500°C for three hours to remove any pre-existing residual stresses.

An elongated denting tool was designed and constructed for the production of 2:1 aspect ratio dents. The design is consistent with that of the circular denting tools used in previous studies. The tool and die (male and female parts, respectively) are shown in Figure 5. The outer dimensions of the tool are 1.55 cm x 3.20 cm, while those for the die are 2.35 cm x 4.20 cm. The tool and die were constructed in the Queen's Physics department machine shop and then sent to an outside facility for heat treatment.



Figure 5. Tool and die used for creating elongated dents in the present study. Note that the tool and die are completely separate items and in this photo, which shows the tool simply resting on the die.

A 50 kN hydraulic press was used to create the dents. The tool is attached to the hydraulic ram using a screw fitting, while the die sits on a support platform below. The 3 mm thick plate samples were placed on the die and the tool was lowered to create dents of varying depths. Dent depths of 3, 4, 5, 6 and 7mm were produced.

A typical test dent is shown in Figure 6. Figure 6(a) shows the topside of the dent, while Figure 6(b) shows the underside.

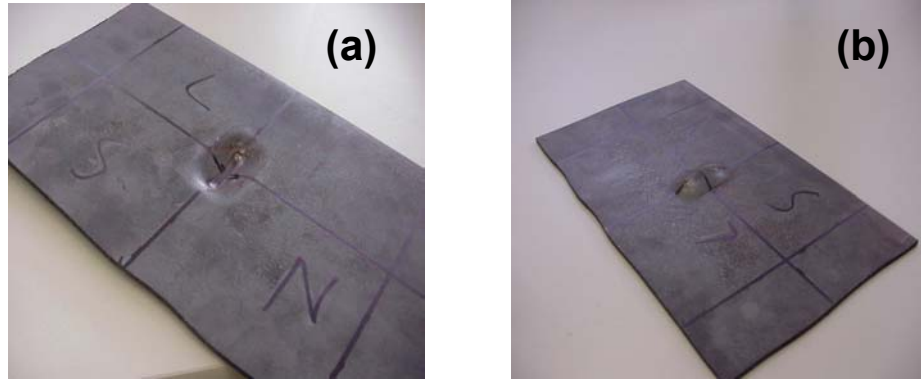


Figure 6. Dent created using the elongated denting tool shown in Figure 5. a) topside of dent, b) underside of dent. Dents were smooth except for localized depressions near the dent ends, associated with the corners of the punch.

### 6.1.3 Experimental Procedures

MFL measurements were made on the topside and underside of the sample. Schematic side views of the Hall probe scan profiles are shown for each of these cases in Figures 7 and 8. When conducting the topside scan (Figure 7) a thin sheet of plastic insulator was placed over the ‘hole’ to keep the Hall probe level with the rest of the plate surface. The plastic insulator had no effect on the magnetic field results. During the underside scans (Figure 8), the sensor arm design allowed the probe to vertically retract and extend, thus following the axial profile of the dent. It is important to note that the Hall probe orientation, which has a significant affect on the shape of the MFL signal, was kept parallel to the sample plane rather than relative to the dent profile as shown in Figure 9. This Hall probe orientation is also consistent with that used in commercial MFL tools.



Figure 7. Illustration of hypothetical data collection points along topside of sample. (Note that this curvature is not intended to reflect the profile of a true dent).



Figure 8. Illustration of hypothetical data collection points along underside of sample.

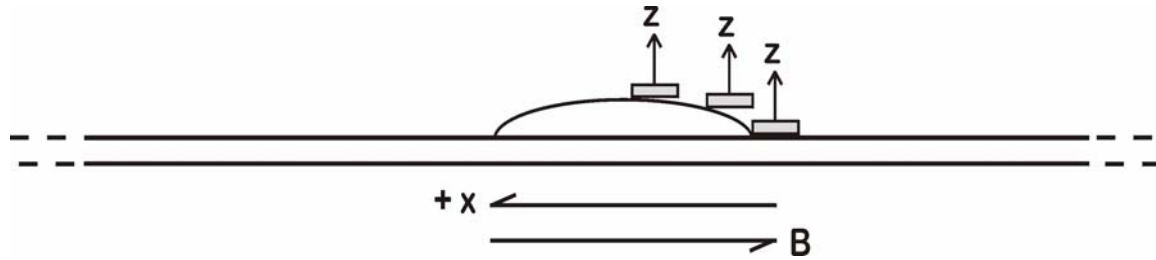


Figure 9. The Hall sensor maintains its orientation parallel to the sample in the x-plane.

In separate experiments MFL scans were made in each of the radial, axial and circumferential direction for each sample. Results from experimental scans were first corrected for background effects, smoothed and finally presented as contour plots. Background subtraction methods were carefully examined in the 2004 study<sup>[9]</sup> to ensure that valuable signal details were preserved. Smoothing, contour and surface plotting of the MFL experimental scan data was done within the software package Surfer<sup>[10]</sup>. Surfer Matrix Smoothing Method 4 was chosen since this method smoothed all of the inconsistent variations in the signals while still retaining the significant features of each plot.

## 6.2 Experimental MFL Results from Elongated Dents

Separate 2:1 dents were produced for measurements in both the axial and circumferential directions, and are termed the axially and circumferentially-oriented dents, respectively, in what follows. For each orientation there were five different dent depths: 3, 4, 5, 6 and 7 mm. Each dent depth sample was measured before and after annealing, and all measurements were made both from the topside and underside configuration. The underside corresponded to a ‘typical’ measurement during an inspection scenario. Finally, for each particular depth, orientation, and measurement configuration, three components of the MFL signal were measured: the radial, axial and circumferential, respectively termed  $MFL_{\text{radial}}$ ,  $MFL_{\text{axial}}$  and  $MFL_{\text{circ}}$ . Ultimately, more than 120 experimental measurements were made during this portion of the study as outlined in Table 1 below.

Table 1

Location	Dent Orientation (2:1)	Dent Depth (mm)	Metal Condition	Measurement Orientation	No. Contour Plots Produced
Topside	Circumferential	3, 4, 5, 6, 7	Before annealing; After annealing	$MFL_{\text{radial}}$ $MFL_{\text{axial}}$ $MFL_{\text{circ}}$	30
Topside	Axial	3, 4, 5, 6, 7	Before annealing; After annealing	$MFL_{\text{radial}}$ $MFL_{\text{axial}}$ $MFL_{\text{circ}}$	30
Underside	Circumferential	3, 4, 5, 6, 7	Before annealing; After annealing	$MFL_{\text{radial}}$ $MFL_{\text{axial}}$ $MFL_{\text{circ}}$	30

Underside	Axial	3, 4, 5, 6, 7	Before annealing; After annealing	MFL <sub>radial</sub> MFL <sub>axial</sub> MFL <sub>circ</sub>	30
-----------	-------	---------------	--------------------------------------	--	----

Because of the large number of 2:1 aspect ratio results, only a select few are included in the main body of the report. The full matrix of 2:1 plots is included on a CD in the appendix of the report. In addition to the 2:1 dent studies, a parallel study of 4:1 aspect ratio dents was conducted in the AMG labs. Select results from the 4:1 dents are included in this report for comparison purposes.

In general, the topside measurements contain features that are similar to the underside results. Therefore, for the purposes of summarizing the main features of the experimental data, Section 5.2 contains a discussion of only underside measurements. Underside scans correspond to scans obtained on the inside wall of a pipe and are therefore similar to those obtained during a typical inspection scenario. Figure 8 in the previous section showed a typical experimental scan to obtain an underside measurement. Data will only be shown for the 3mm and 7mm dent depths, which represent the shallowest and deepest dents studied. Overall, a subset of 24 plots of MFL signals from the underside of 2:1 elongated dents are presented in this section.

Prior to considering the elongated dent results obtained in the current study, it is helpful to examine the results obtained for the MFL<sub>radial</sub> component for 40-mm diameter circular dents evaluated in the previous study. Figure 10 shows these results, for 3-mm and 7-mm dents, before and after annealing.

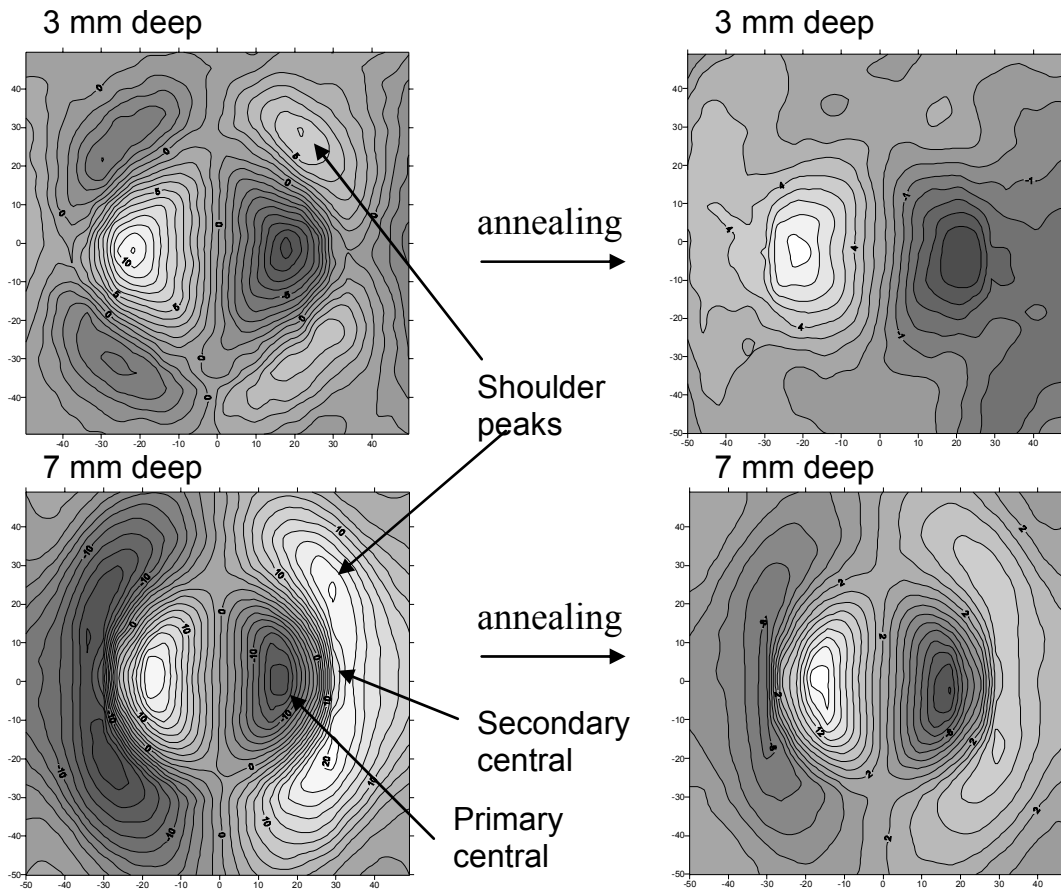


Figure 10.  $MFL_{radial}$  plots for 40mm diameter circular dents of 3mm and 7mm depths, before and after annealing.

The main features of these plots are:

- Shoulder peaks, which are generally associated with residual stress from denting, diminish considerably after annealing; and
- Primary and secondary central peaks, which are associated with the dent geometry, remain relatively unchanged after annealing.

Of specific interest are the shoulder peaks, which, from annealing studies and magnetic FEA analysis, appear to be associated with residual stresses in the dent rim. Both the primary and secondary central peaks have been shown to be associated with dent geometry using magnetic FEA modeling. (See Figure 3 in Section 2. The primary and secondary central peaks are also present in Figure 2, particularly in the deeper dent.) The primary central (geometry) peak is present in all dent results, however the secondary central peak is usually somewhat obscured in shallower dents and becomes more prominent with depth. In deeper dents, the secondary central peak usually extends to the stress shoulder peak as seen in the 7mm deep dent in Figure 10. Since the stress shoulder peak and the secondary central geometry peak tend to coincide, it is often difficult to evaluate exactly how much the stress peak decreases upon annealing.

The elongated 2:1 dents will be discussed on the following pages, with the circular dent signals of Figure 10 referred to for comparison purposes. In the discussion that follows, the  $MFL_{\text{radial}}$  results will be considered first for both circumferential and axially-oriented 2:1 dents, followed by the  $MFL_{\text{axial}}$  and finally the  $MFL_{\text{circ}}$  results.

### 6.2.1 $MFL_{\text{radial}}$ Results: 2:1 Elongated Dents - Underside Scans

The following pages contain the underside scan results for the  $MFL_{\text{radial}}$  component of the axially-oriented (Figure 11) and circumferentially-oriented (Figure 12) dents. These can be compared directly with the  $MFL_{\text{radial}}$  results for the circular dents, shown in Figure 10, keeping in mind that the elongated dents are about half the ‘width’ of the circular dents.

Qualitatively, all of the significant features seen in the circular dent  $MFL_{\text{radial}}$  results are also observed for the 2:1 dents in both orientations. The stress-related shoulder peaks are clearly seen in both shallow (3mm) dents of Figures 11 and 12, however, as expected they are closer together in the axially-oriented dent. The fact that they lie closer together in the axially-oriented case means that they are almost completely obscured by the secondary central peak as the dent becomes deeper (Figure 11, 7mm deep dent). This is not the case for the circumferentially-oriented dent, where these stress shoulder peaks are clearly separated.

Figure 13 examines how the  $MFL_{\text{radial}}$  peak-to-peak values change as a function of dent depth, for the primary central peak (shown on left) and the shoulder peaks (shown on right). These measurements are somewhat difficult to quantify for the case of the shoulder peaks, since the shoulder peaks nearly always coincide with the secondary central (geometry) peak. The plots are shown before and after annealing. The points to note from these plots are the following:

- The central primary peak results are fairly similar for the axial and circumferential results – the peak height does not appear to change much with defect depth and also changes little with annealing, indicating that the residual stresses associated with the dent base are relatively small. Interestingly this central primary peak grows slightly with annealing in the circumferentially-oriented dent case, suggesting that the residual stress peak was the opposite polarity and therefore caused a decrease in the overall peak height.
- The stress shoulder peaks tend to be somewhat higher in magnitude than the central geometry peak and increase in size with increasing defect depth, although this is likely due to the fact that they lie on top of the secondary central peak.
- The stress shoulder peaks drop quite considerably in magnitude with annealing. This is expected since the residual stresses should be removed with the annealing procedures.



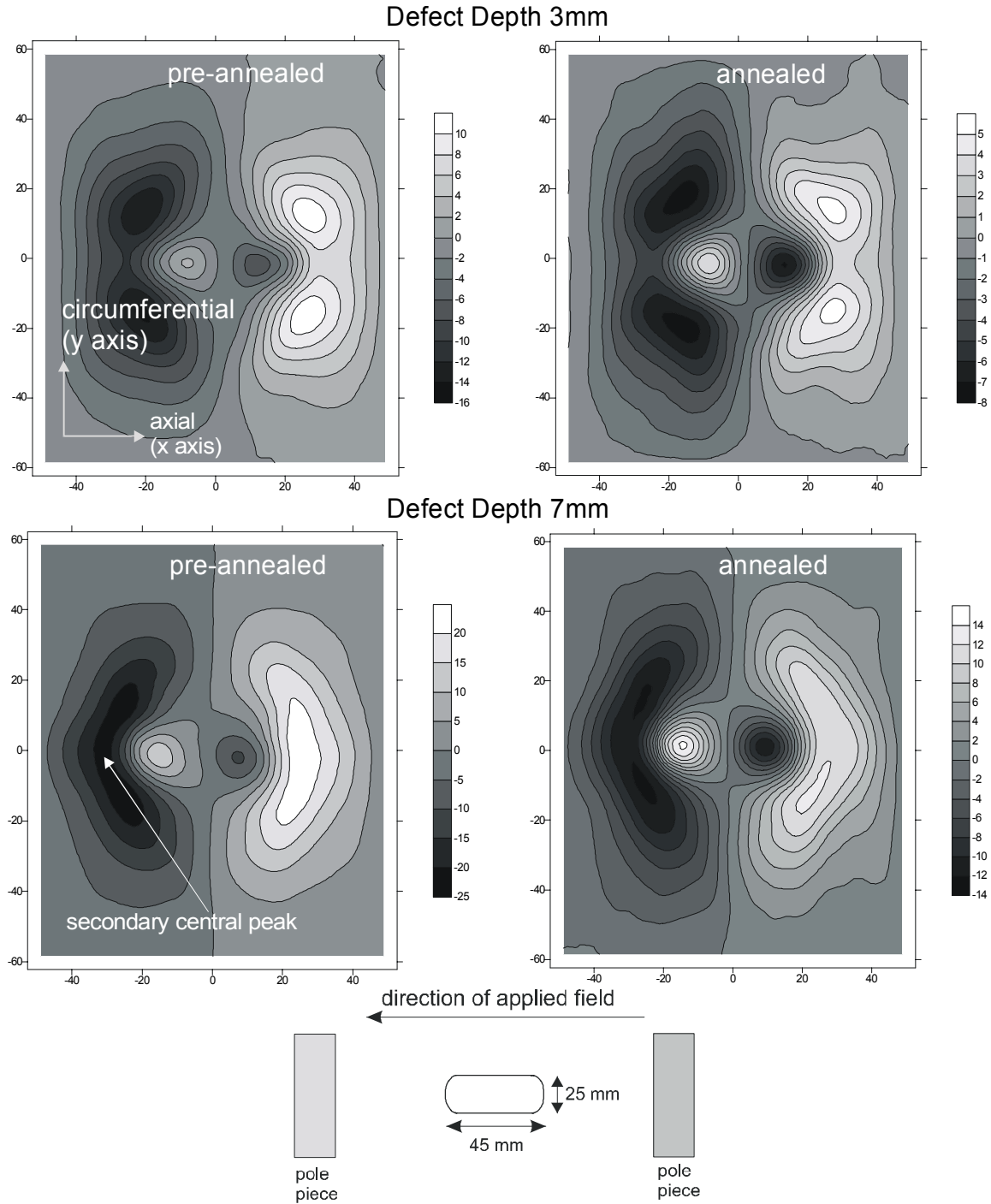


Figure 11. Preannealed and annealed underside MFLradial result for axially-oriented dent. Note that MFL scales are different for each plot. Results are displayed for 3 mm and 7 mm deep dents. In the 7-mm dents, the secondary central features are prominent and appear to “cover” the shoulder. MFL signal is in units of  $10^{-4}$  Tesla.

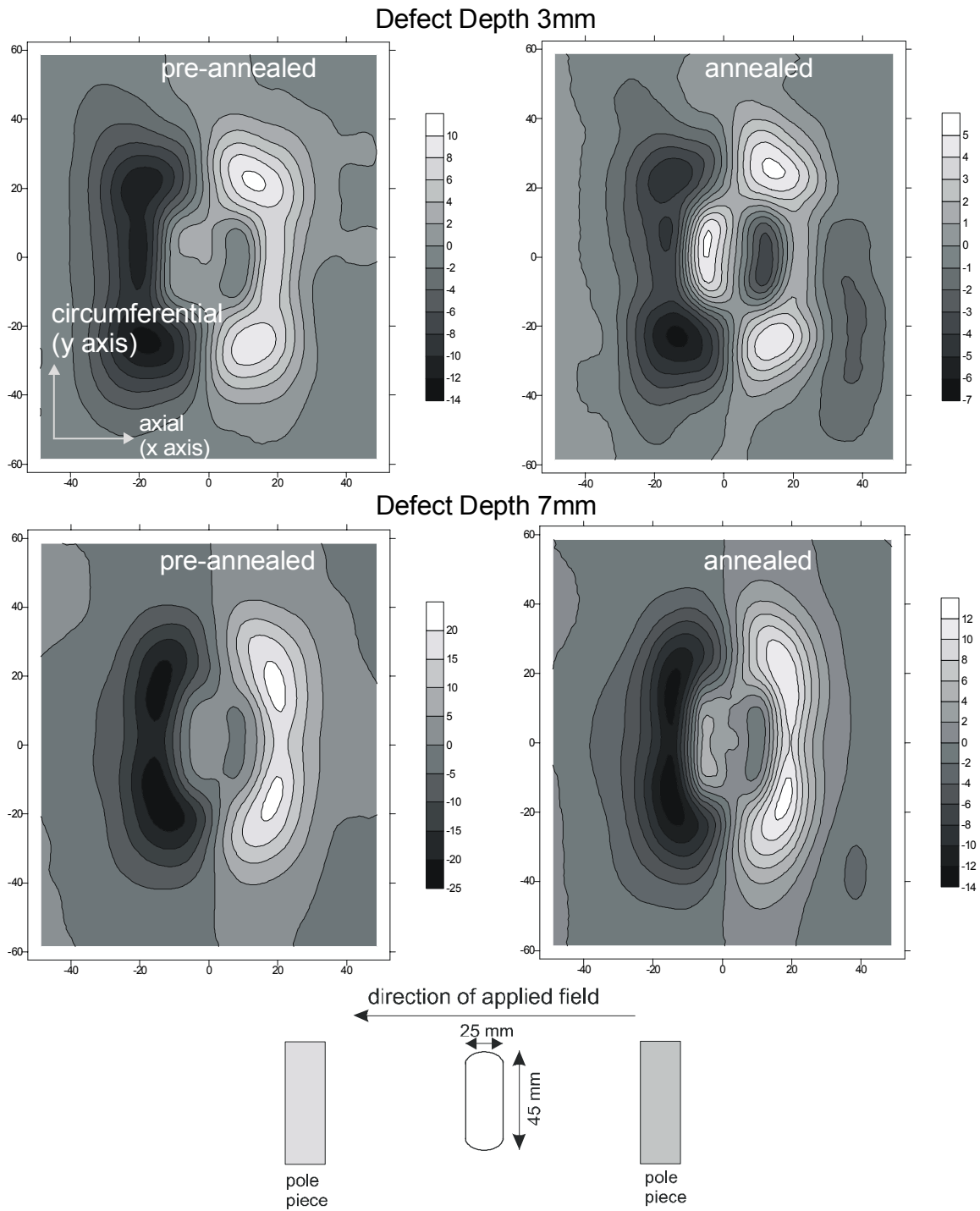


Figure 12. Preannealed and annealed underside MFLradial result for circumferentially-oriented dent. Note that MFL scales are different for each plot. Results are displayed for 3mm and 7 mm deep dents. MFL signal is in units of ( $10^{-4}$  Tesla).

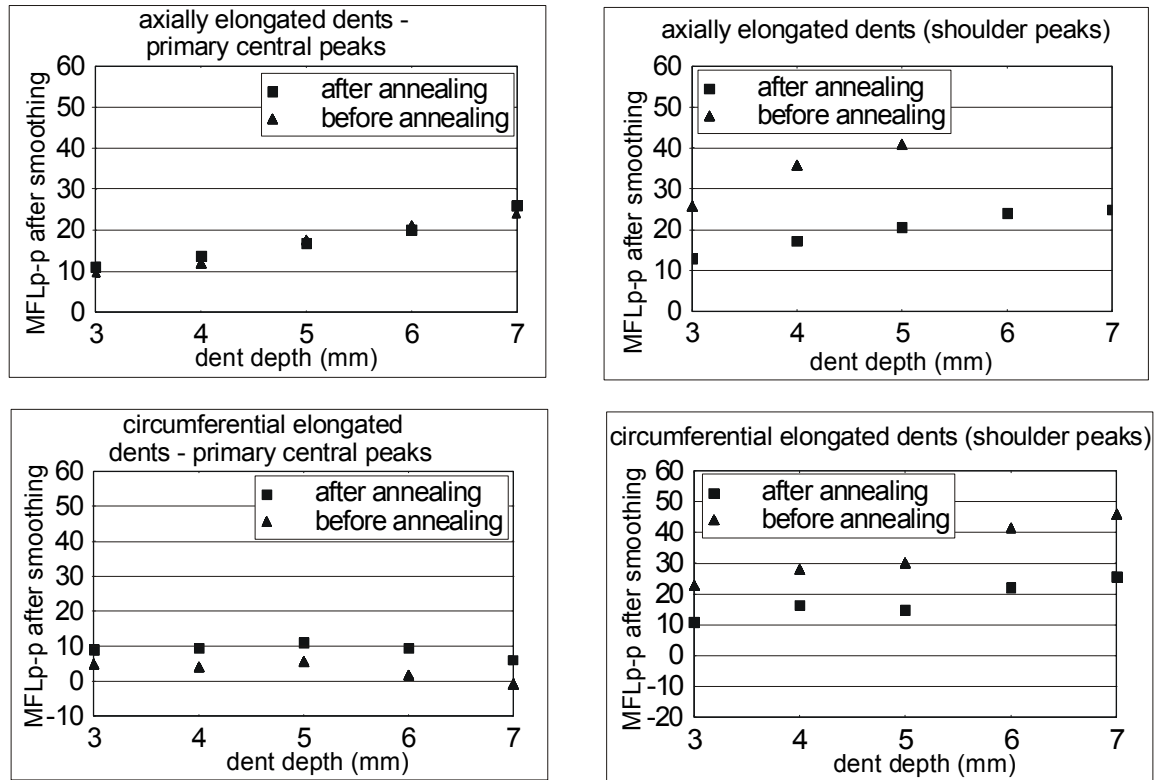


Figure 13. MFLradial peak to peak results from the underside of the dent before and after annealing. Missing data points are due to the fact that there was too much overlap to distinguish individual peaks. The negative trend of MFL signal with dent depth for circumferentially oriented dents is not clearly understood at present.

### 6.2.2 MFL<sub>axial</sub> Results: 2:1 Elongated Dents, Underside Scans

The following two pages contain the underside scan results for the MFL<sub>axial</sub> component of the axially-oriented (Figure 14) and the circumferentially-oriented (Figure 15) dents. It is important to note that the MFL<sub>axial</sub> component is normally used in commercial pipeline inspection tools for defect identification and sizing.

Figure 14 shows that the axially-oriented dent MFL<sub>axial</sub> signal is characterized by only central peaks, specifically, two positive-polarity, side central peaks and a broad central peak that is slightly negative. Similar results (not shown) were also seen in the circular dent samples. With increasing dent depth, these features become more pronounced but otherwise do not change. Interestingly, the plots for the dents exhibit nearly the same features as a corrosion pit of the same dimensions and orientation. (Shown at the bottom right of the page in the inset is an MFL<sub>axial</sub> plot for a through-wall pit of the same axial orientation.). It should be noted that this similarity may lead to problems with dent identification and discrimination in practice since a dent signal may be misinterpreted as an elongated pit signal when only the MFL<sub>axial</sub> component of the measurement is evaluated.

Figure 15 shows the  $MFL_{axial}$  signal for a circumferentially-oriented dent. The  $MFL_{axial}$  signal is elongated in the circumferential direction compared to the axially oriented dent result of Figure 14. Additionally, a second set of ‘shoulder peaks’ is clearly seen at the top and bottom of the plot.

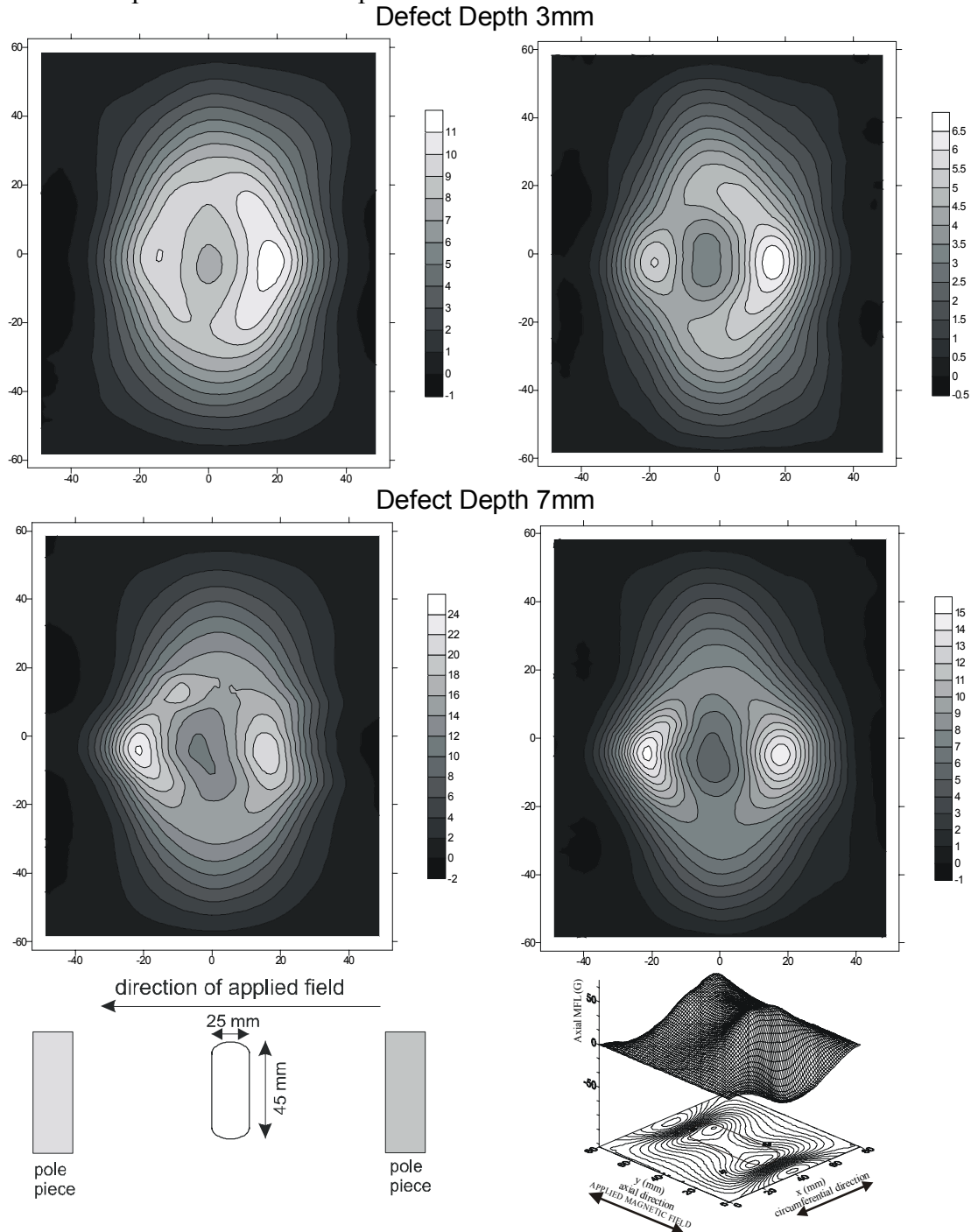


Figure 14. Pre-annealed and annealed underside  $MFL_{axial}$  result for axially-oriented dent. Results are displayed for 3 mm and 7 mm deep dents. Note that MFL scales are different for each plot. MFL signal is in units of ( $10^{-4}$  Tesla).

Shown at the bottom right of the figure is an  $MFL_{axial}$  plot for an axially-elongated corrosion pit. Comparing this plot to those for the dents indicates that similar features are present.

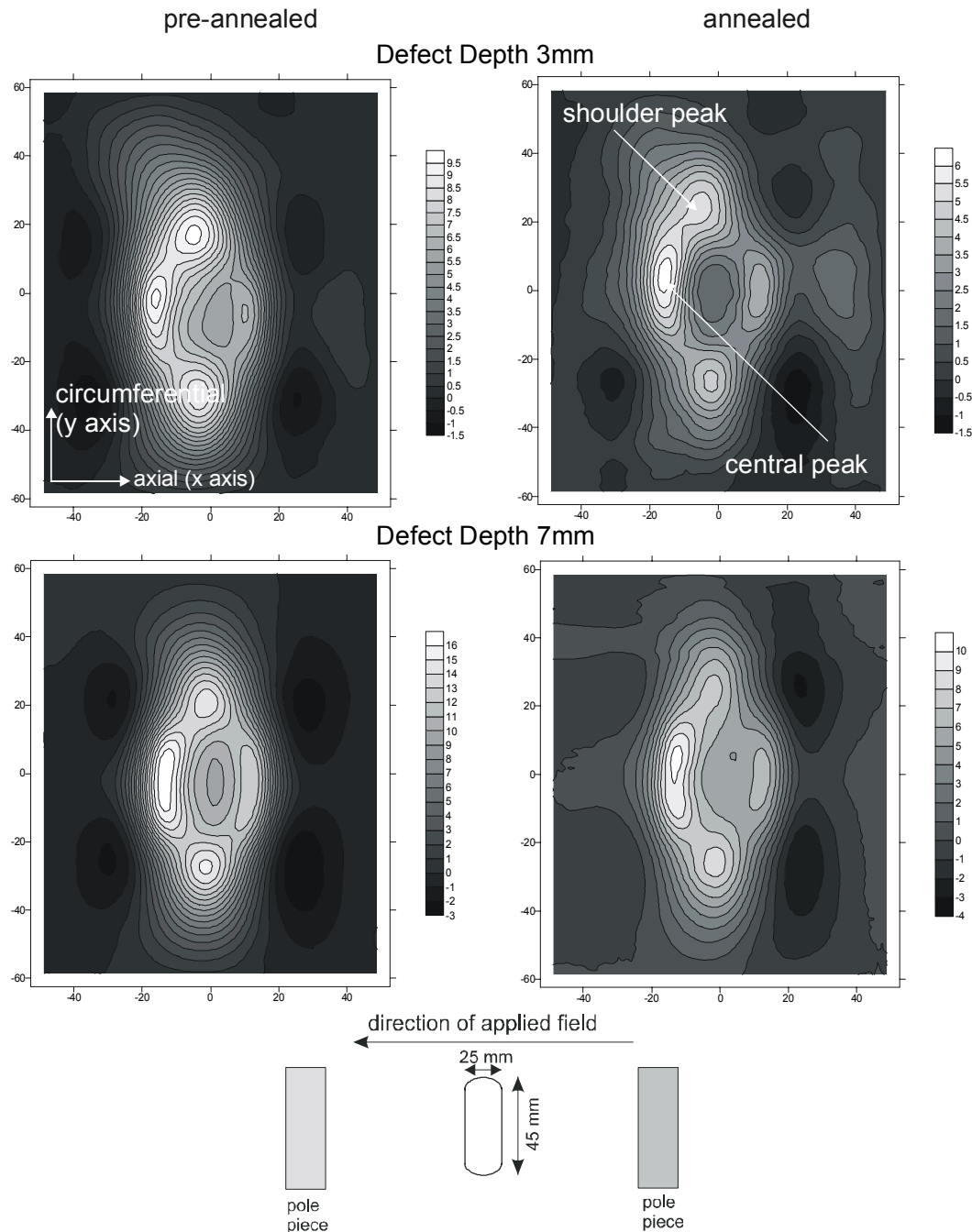


Figure 15. Preannealed and annealed underside  $MFL_{axial}$  result for circumferentially-oriented dent. Note that MFL scales are different for each plot. Results are displayed for 3 mm and 7 mm deep dents. The axial peaks that are due to the same flux leakage that creates the radial central peaks in Figure 12 are referred to as shoulder peaks. MFL signal is in units of ( $10^{-4}$  Tesla).

Figure 16 examines how the  $MFL_{axial}$  peak-to-peak values change as a function of dent depth. For the axially-oriented dent, the  $MFL_{axial}$  peak height increases only gradually with dent depth and does not change significantly after annealing, indicating that the residual stress effects on the  $MFL_{axial}$  signal are small for this axial orientated defect configuration. There is no shoulder peak for this case.

For the circumferentially-oriented dent, the overall peak size is greater than for the axially-oriented dent. There is a slight depth dependence for both the central and shoulder peaks. Furthermore, both central and shoulder peaks decrease with annealing, although the shoulder peaks show a more significant reduction, consistent with the fact that they are associated with strain.

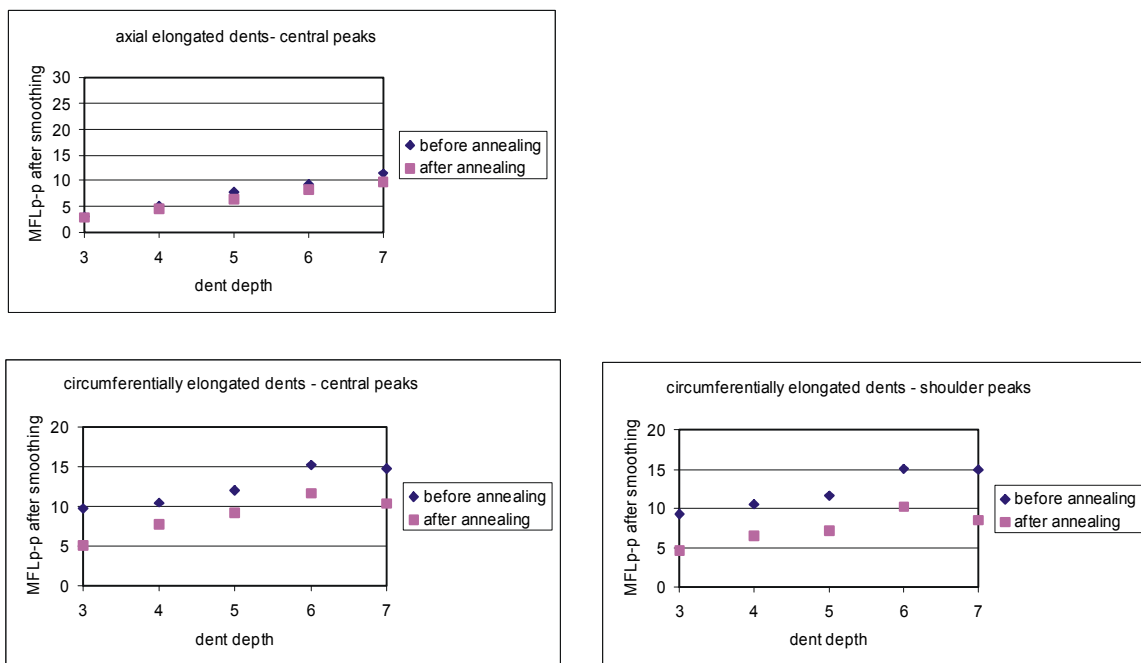


Figure 16.  $MFL_{axial}$  peak to peak results – underside, before and after annealing. As in Figure 13 the central peak MFL magnitudes for circumferentially elongated dents display a slight negative MFL signal trend with dent depths, which is not clearly understood as yet.

Overall, the results tend to indicate that the  $MFL_{axial}$  signal component may not be entirely suitable for dent discrimination and characterization since the axial dent configurations examined in this study produce signals that are similar to those produced for axially-elongated corrosion pits. This is not the case for the  $MFL_{radial}$  component, which has a number of distinct, additional and distinguishable features compared to a typical  $MFL_{radial}$  signal derived from a corrosion pit.

### 6.2.3 MFL<sub>circ</sub> Results: 2:1 Elongated Dents, Underside Scans

The following pages contain underside scan results for the MFL<sub>circ</sub> component of the axially-oriented (Figure 17) and circumferentially-oriented (Figure 18) dents.

Figure 17 shows that the axially-oriented dent MFL<sub>circ</sub> signal is characterized by a number of peaks. In fact, the four central peaks are produced, which is similar to those observed for elongated corrosion pits. (The inset diagram at the bottom of Figure 17 shows a typical MFL<sub>circ</sub> signal for an axially-elongated corrosion pit.). However the axially-elongated dent MFL<sub>circ</sub> signals in Figure 5.17 indicate that additional ‘shoulder’ peaks are also present which are normally not observed for corrosion pits. All peaks – the four central and the four shoulder peaks produced for the dent, appear to become more distinct with increasing depth. The shoulder peaks diminish considerably with annealing and are therefore likely associated with residual dent stresses.

Figure 18 shows the MFL<sub>circ</sub> signals from circumferentially-elongated dents. Again, four central peaks and four shoulder peaks are observed, although the overall signal is elongated in the circumferential direction, when compared to that observed for the axially-elongated dents. As in the case of the axially-oriented dents, all peaks appear to increase with increasing dent depth. However, in this case annealing appears to decrease all peaks (central and shoulders) quite significantly.

Finally, Figure 19 summarizes the results of all of the peak height values with depth before and after annealing. There appears to be a moderate dependence of peak height with depth for all peaks. The MFL<sub>circ</sub> signal peaks appear to diminish with annealing for all cases.

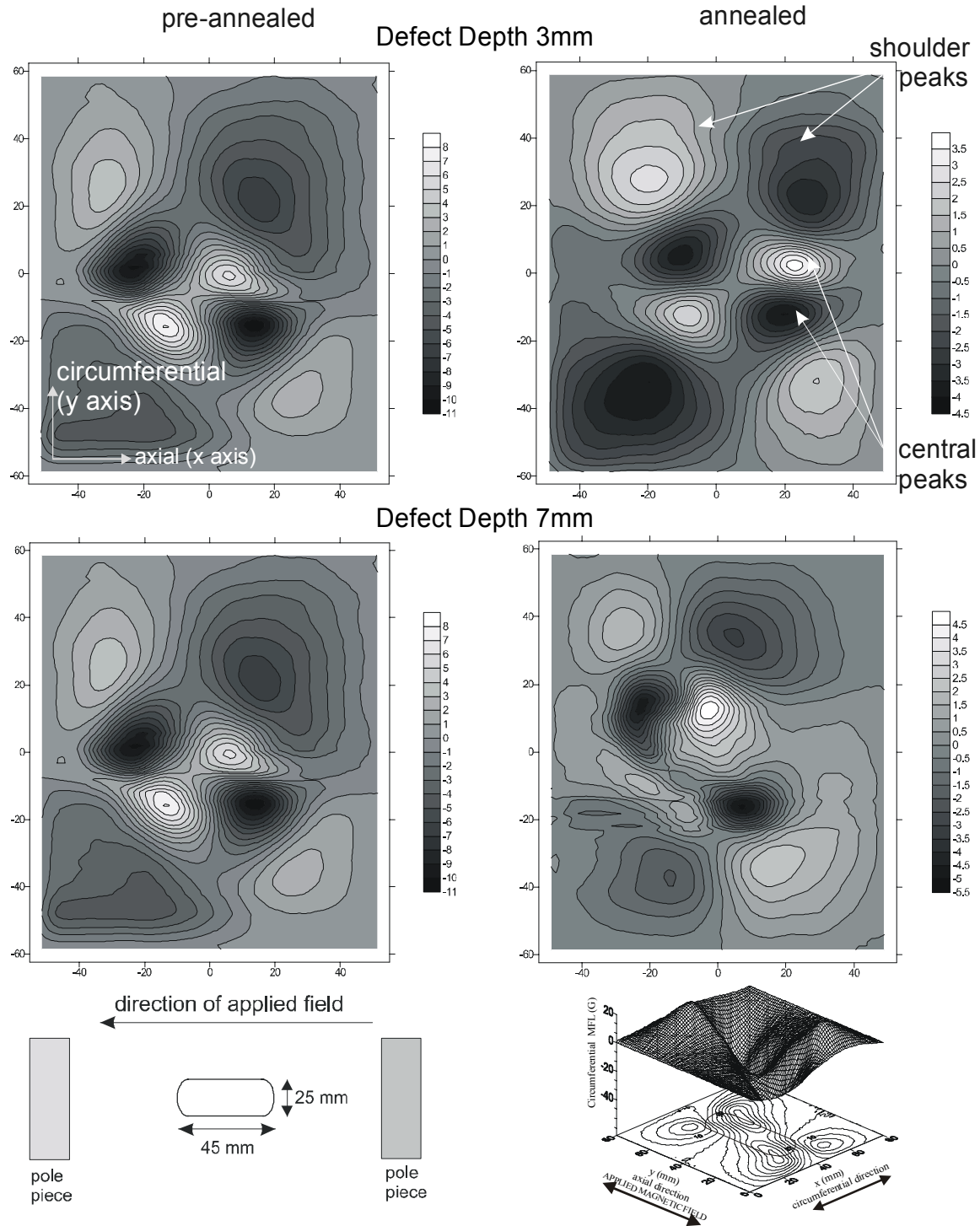


Figure 17: Preannealed and annealed underside MFLcirc result for axially-oriented dent. Note that MFL scales are different for each plot. Results are displayed for 3 mm and 7mm deep dents. MFL signal is in units of  $(10^{-4}$  Tesla). At the bottom right of the figure is shown a typical MFLcirc plot for an axially-elongated corrosion pit. The 4 peaks here are similar to the 4 central peaks in the dent plots.



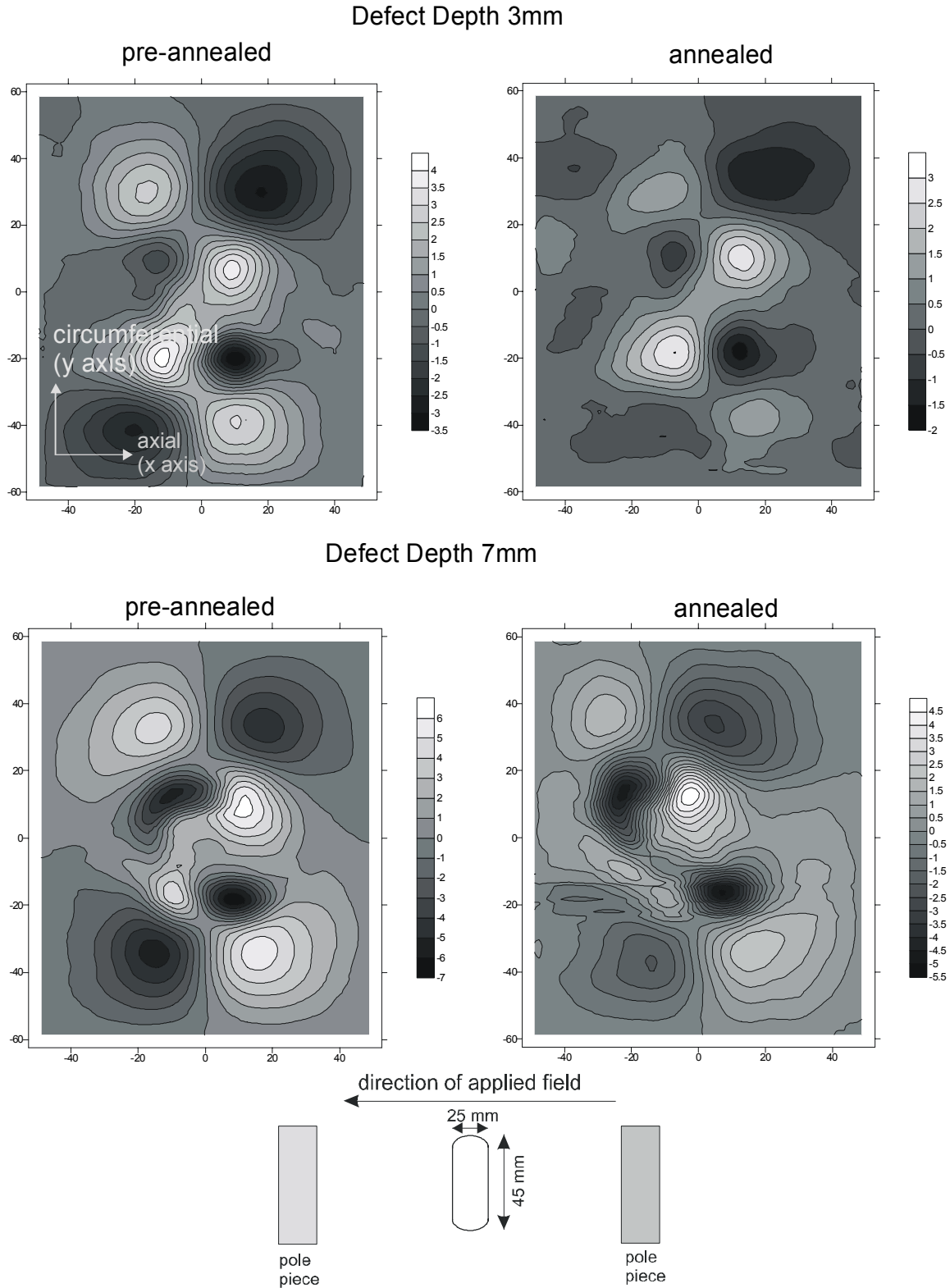


Figure 18: Preannealed and annealed underside MFLcirc result for circumferentially-elongated dents. Note that MFL scales are different for each plot. Results are displayed for 3 mm and 7 mm deep dents. MFL signal is in units of ( $10^{-4}$  Tesla).

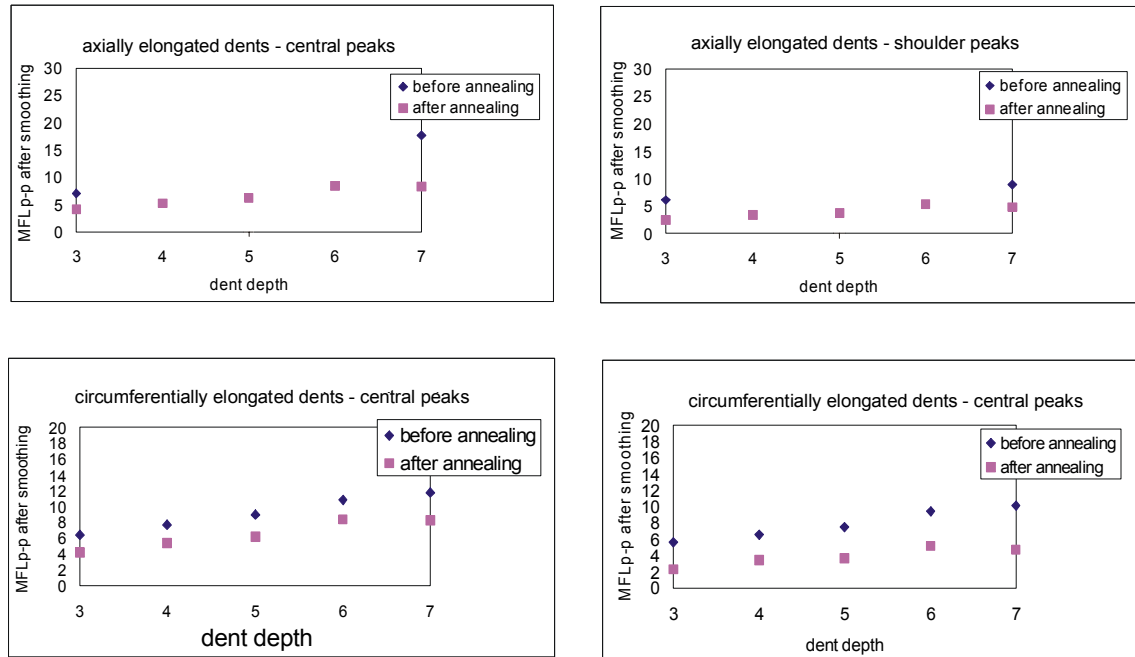


Figure 19. MFL<sub>circ</sub> peak to peak results, underside, before and after annealing. As in Figure 13 the central peak MFL magnitudes for circumferentially elongated dents display a slight negative MFL signal trend with dent depths, which is not clearly understood as yet.

#### 6.2.4 Comparison of All Experimental Results, $MFL_{radial}$ , $MFL_{axial}$ , $MFL_{circ}$

Comparison of the results presented in Figures 11-19 indicates the following:

- Comparison of the peak-to-peak values for the  $MFL_{radial}$ ,  $MFL_{axial}$  and  $MFL_{circ}$  cases in Figures 13, 16, and 19 indicates that the  $MFL_{radial}$  component signal has the highest overall magnitude. This is to be expected since the detector for the radial component measurement sits closer to the surface than for the axial and circumferential cases... Consequently, more detailed information is likely to result from an examination of the  $MFL_{radial}$  component compared to the  $MFL_{axial}$  and  $MFL_{circ}$  components.
- The  $MFL_{radial}$  and  $MFL_{circ}$  component signals show distinct residual stress and geometry-related features. This is not the case for the  $MFL_{axial}$  component, where the signal for the axially-oriented dents appears similar to that produced for an axially-oriented corrosion pit.
- In general all features (central and shoulder peaks) tend to diminish only slightly with annealing; suggesting that the residual stress affects the entire signal to a small extent. However, in most cases (e.g. the  $MFL_{radial}$  component signal) the shoulder peaks diminish considerably with annealing, again suggesting that the shoulder peaks are strongly residual stress-related.

### 6.3 Structural FEA Modeling Results

Since the MFL signals are affected not only by the geometry of dents but also by the presence of strain in the dented region, it is necessary to obtain information about the strain patterns associated with denting. As mentioned earlier, it is the elastic residual strain that affects MFL signals. The first stage of the modeling work, therefore, involved studying the elastic residual strain patterns around a dent using structural finite element modeling and analysis. A nonlinear structural FEA model using ANSYS<sup>[12]</sup> was used to obtain predictions of the three-dimensional residual stress profiles in a dented plate.

A diagram of the modeled denting tool and die, with the plate in place, is shown in Figure 20. The model tool and die dimensions shown are the same as those used for the experimental 2:1 aspect ratio dents discussed in Section 5.1. The die was rigid and the plate was not clamped at its edges. The punch stroke depth was 4mm, after which the tool was removed and the residual stress/strain analyzed (note that the other depths were not modeled, since only qualitative results were required and the 4mm depth was expected to be representative of the range from 3-7mm). Only one-quarter of the model was considered due to symmetry considerations. The interfaces between the die and the plate and between the plate and the punch were modeled using an automatically generated surface-to-surface contact algorithm within Ansys that uses the material properties of both contacting surfaces to calculate the stiffness of the contact elements. An elastic Coulomb friction law was assumed and a friction coefficient of 0.15 was assigned to the contacting surfaces. The stress-strain behavior of the steel was described by a bilinear total stress-total strain curve starting at the origin and with positive stress and strain values. A piecewise linear elastic perfect plastic material model was assumed for the plate with following parameters: Young's modulus = 207 GPa, yield strength = 160 MPa, tangent modulus = 0.112 GPa, Poisson's ratio = 0.290, and density = 7900 kg.m<sup>-3</sup>.

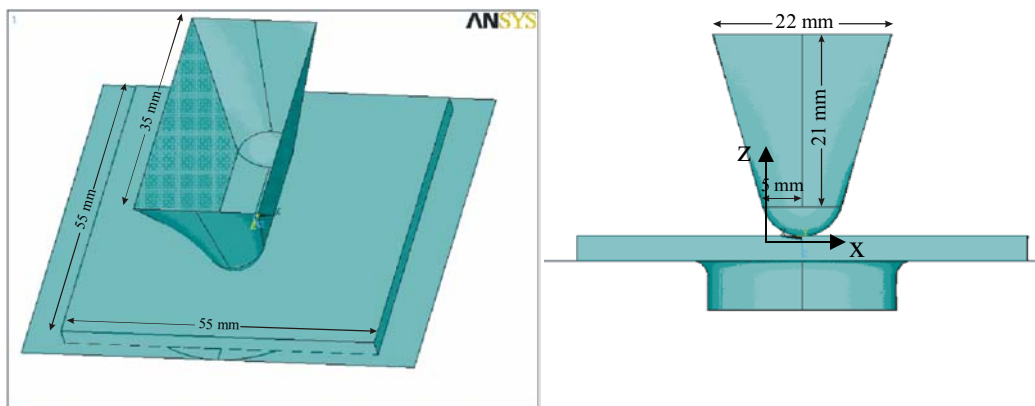


Figure 20: The modeled tool, die and plate used for obtaining the residual stress patterns for elongated dents in the present study.

After the tool was removed in the model, the residual stress distributions were analyzed in the plate. Figures 21, 22 and 23 show the residual normal stress patterns for the x, y, and z directions with the 4mm dent sectioned through the middle to view the stress distribution through the thickness. Figure 24 shows the residual shear stress distribution for the full dent (not sectioned).

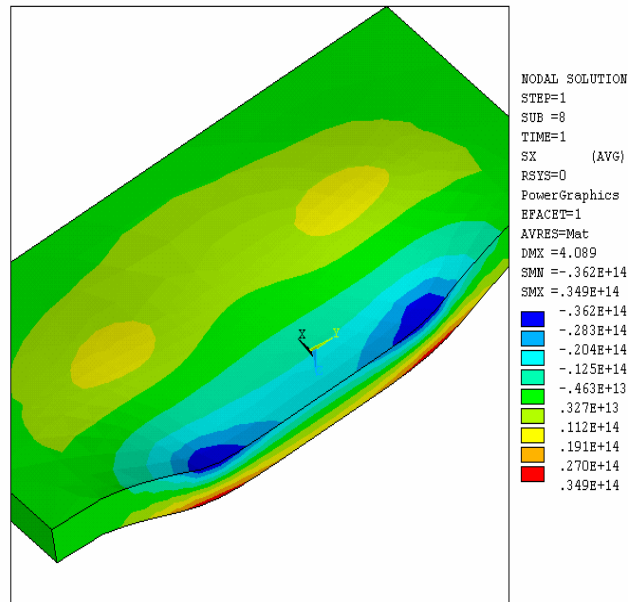


Figure 21. Residual normal stress in the x direction for a 2:1 aspect ratio, 4mm deep dent. The dent is sectioned through the centre to show the stresses through the wall thickness. The scale on the right indicates stress in Pa.

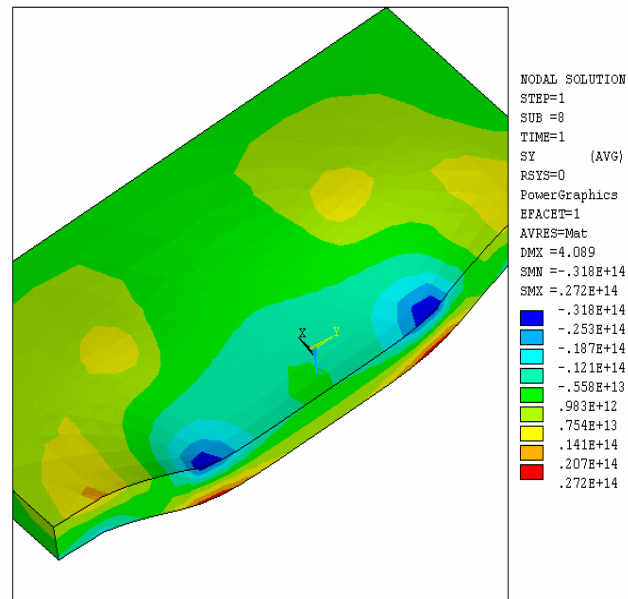


Figure 22. Residual normal stress in the y direction for a 2.1 aspect ratio, 4mm deep dent. The dent is sectioned through the centre to show the stresses through the wall thickness. The scale on the right indicates stress in Pa.

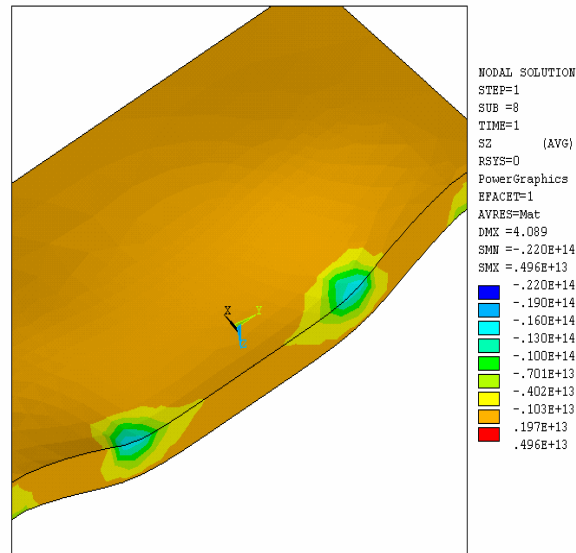


Figure 23. Residual normal stress in the z (through-wall) direction for a 2:1 aspect ratio, 4 mm deep dent. The dent is sectioned through the centre to show the stresses through the wall thickness. The scale on the right indicates stress in Pa.

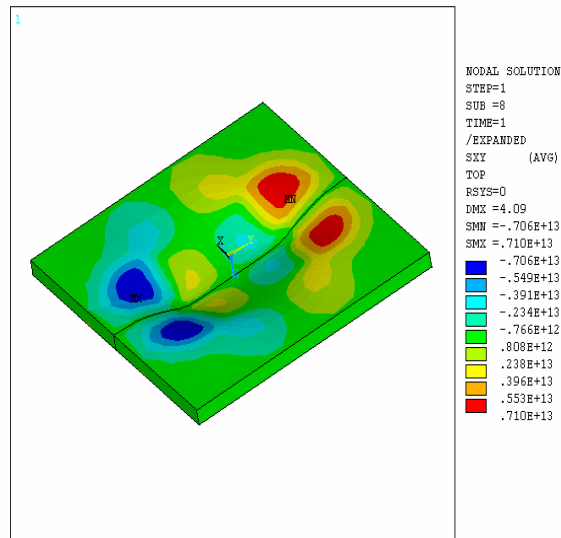


Figure 24. Residual shear stress in the xy plane for a 2:1 aspect ratio, 4mm deep dent. The scale on the right indicates stress in Pa.

High compressive x stresses occur near the dent base at the two extremes on the topside (Figure 21) and high tensile x stresses occur at similar locations on the underside. Comparatively weak tensile and compressive x stresses occur at other locations near the dent rim. The y stress pattern (Figure 22) is quite similar to the x pattern, particularly near the dent base. However, in the peripheral region, it is slightly different from that of the x. Z direction stresses (Figure. 23) are much smaller in magnitude compared with those in the other directions.

Figure 24 shows the topside shear stress patterns. The underside pattern is similar but of opposite sign. The regions of interest are the high stress shoulder regions that cover the dent base and rim areas. In Figure 24 the positive shear stress peak is located at approximately at  $65^\circ$  to the y plane. As will be discussed later, knowledge of the magnitude and polarity of normal x, normal y, and shear stresses is vital for the magnetic FEA model. The normal z stresses, being perpendicular to the flux path and comparatively small, are unlikely to play a significant role.

Finally, earlier work<sup>[9]</sup> has shown that the effect of stresses existing in the direction of the applied magnetic field is overshadowed by the effect of the magnetic field itself. Since the applied field in this case is axial, any stress in this direction is expected to have little or no effect on the MFL signal. As a result, in the discussions that follow only shear stresses and normal stresses perpendicular to the applied field direction will be incorporated into the magnetic FEA model.

#### **6.4 Magnetic FEA Modeling and Residual Stress Incorporation Using Magnetic Anisotropy Variations**

Infolytica's MagNet6 software is used for magnetic FEA modeling. The quarter symmetry of the dent allows the use of a quarter model as shown for the axially-oriented dent in Figure 25. Note that, in magnetic modeling, the word 'axial' means in the x-direction (direction of the applied magnetic field), 'circumferential' means in the y-direction (in the plane of the sample plate), and 'radial' means normal to the plane of the sample. The quarter model consists of a steel plate with a quarter dent at the lower left corner as shown. The quarter dent is 32 mm long (x direction) and 16 mm wide (y direction), thus having an aspect ratio of 2:1. Note that in this figure, the x-axis is aligned with the long dimension of the dent, which differs from the convention used in Section 5.3.

As seen in Figure 25, the dent is comprised of the almost planar 'dent base' region at the dent center and the outer 'dent rim' region that includes 'dent wall' as well as a part of the undeformed plate just beyond the periphery of the dent (i.e., the transition region from the dent base to the undeformed wall thickness). The model is divided into a number of different segments around the dent and through the thickness. In total, there are 112 segments in this model. The segments can be assigned different magnetic permeability functions in each of the three orthogonal directions to simulate residual stresses that corresponding to the structural FEA results. The circumferentially-oriented dent is identical to that shown in Figure 25 except that the long axis of the dent is perpendicular to the magnet.

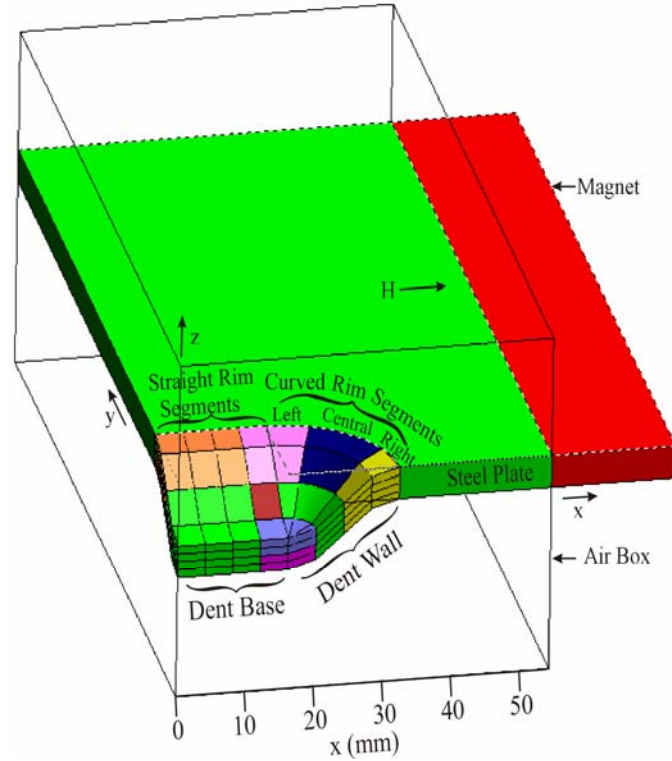


Figure 25. Quarter model of the elongated dent, used for magnetic finite element modeling. The axially-oriented elongated dent is shown here.

Since steel, in general, has a positive magnetostriction coefficient, 180° domains will tend to align their magnetic-easy axes closest to, and ultimately rotate towards, the direction of the applied tensile stress. This increases the magnetic permeability in the tensile stress direction. Conversely, an applied compression will increase the magnetic permeability in a direction transverse to the stress axis.

The Infolytica MagNet6 software allows for 3D non-linear anisotropic FEA calculations with user-defined magnetization functions, which our group has determined in earlier studies<sup>[9]</sup>. Since high axial fields are used, it is assumed that magnetization must always be in the field direction, and that it can be described as an arc tangent of the field, with the  $B$ - $H$  curve approximated as:

$$B = \mu_0 \left[ \frac{2M_s}{\pi} \tan^{-1}(H / H_k) + H \right] \quad (1)$$

where  $\mu_0$  is the permeability of free space,  $H_k$  is a directionally dependent anisotropy parameter,  $M_s$  is the saturation magnetization equal to 1,700 kA.m<sup>-1</sup> (for this steel), and  $H$  is assigned to be 27,500 A.m<sup>-1</sup>. This equation is used to calculate the components of  $B$  by assigning values of  $H_k$  in each of the three orthogonal directions.

Using Eq. (1), the maximum permeability  $\mu_m$  can be shown to be:

$$\mu_m = \mu_0 \left( \frac{2M_s}{\pi H_k} + 1 \right) \quad (2)$$

Thus, smaller values of  $H_k$  imply higher permeability.

Since tensile stress increases, and compressive stress decreases the permeability in the stress direction, the value of  $H_k$  is varied in a specific (x, y, or z)\* direction to simulate applied stress. For example, one can simulate a tensile stress in the y direction by decreasing  $H_k$  in that direction and/or by increasing  $H_k$  along the other two orthogonal directions. In general, the anisotropy parameter in any given direction is expressed as:

$$H_k = H_{kx}\alpha_x^2 + H_{ky}\alpha_y^2 + H_{kz}\alpha_z^2 \quad (3)$$

where  $H_{kx}$ ,  $H_{ky}$  and  $H_{kz}$  are the three orthogonal anisotropy parameters, and  $\alpha_x$ ,  $\alpha_y$ , and  $\alpha_z$  are the cosines of the field vector in that direction.

The exact values of  $H_k$  used in this model were determined in earlier experimental studies<sup>[2]</sup> that examined the stress and magnetization tensor values for various combinations of applied stress and magnetization direction. In the present study, for the stress-free case, a value of  $H_{k(xy z)} = 9,000 \text{ A.m}^{-1}$  was assigned to all three directions in all the segments of the model (the undeformed ‘background’ plate and the dent segments).

In models where stress was considered, tensile and compressive stresses were incorporated into individual dent segments by assigning  $H_{k(xy z)}$  values that were lower or higher, respectively, than  $9,000 \text{ A.m}^{-1}$ . The values of  $H_{kx}$ ,  $H_{ky}$ , and  $H_{kz}$  for these segments were determined on the basis of the structural FEA residual stress results discussed in Section 5.3.

It should be noted that MFL modeled results can be obtained at either the topside or the underside of the plate or pipe. However, as discussed in earlier sections, the results at the topside are less relevant to commercial inspection practice, since all inspections are conducted internally. Thus, in the modeling results reviewed in Sections 5.5, 5.6 and 5.7 that follow, only the underside MFL results are presented. Additionally, although all three MFL components can be extracted from the model, for brevity only the radial result will be presented in detail.

Finally the MFL<sub>radial</sub> signal is obtained by plotting flux density  $B_z$  at a distance 0.5 mm above (or below) the plate surface, a distance which is consistent with a typical stand-off distance for the radial MFL component signal measurement. However, when analyzing underside MFL signals, the patterns cannot be taken from a single xy plane because of the curved geometry of the dent. In order to account for the fact that, in reality, the Hall sensor has to travel over the dent contour as shown in Figures 8 and 9, data points were extracted from a number of parallel planes located between  $z = -4.5$  to

---

\*Here, the x, y, and z directions correspond to the axial, circumferential and radial directions, respectively.



$z = -12.5\text{mm}$  and a Matlab<sup>[13]</sup> program was used to create an MFL contour plot from those points that lie at a distance of 0.5 mm below the dent contour.

## 6.5 Magnetic FEA Modeling Results: Axially Elongated Dents

### 6.5.1 Axially-Elongated Dent: “Background” No Dent, No Stress Case

All MFL signals, whether obtained in the lab or during a commercial inspection scenario, are background-subtracted. Modeled results must also be background-subtracted in order to highlight MFL features associated with defects. To obtain the MFL background level for the current model it was first necessary to model an undented and unstressed plate having a uniform thickness of 4mm. The  $\text{MFL}_{\text{radial}}$  component results of this model are shown in Figure 26. The dent geometry, including the larger dent rim regions, is superimposed on the top diagram for reference, and it can be seen that the dent lies in the region where the background level is fairly constant. Furthermore, the ‘no dent no stress’ pattern is fairly smooth over the dented region sketched with broken lines. The smoothness is clearly visible from the surface plot. In the modeled results that follow, this background has been subtracted from all plots before presentation.

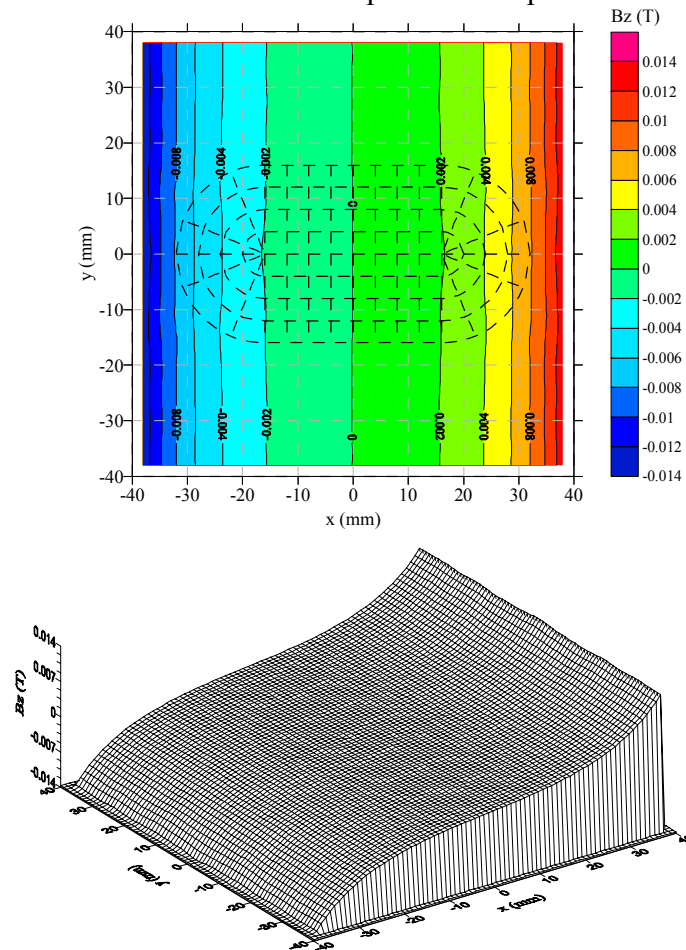


Figure 26. Contour map (top) and surface plot (bottom) of the  $\text{MFL}_{\text{radial}}$  component for the ‘no dent no stress’ (background) case obtained by magnetic FEA modeling.

### 6.5.2 Axially-Elongated Dent: Geometry Only Case

To obtain the “geometry only”  $MFL_{\text{radial}}$  contour plot, a 4-mm deep dent of the shape shown in Figure 25 in Section 5.4 was used. Because this case considers only the geometry contribution to the signal, all of the segments in Figure 25 are considered to have zero stress, and are assigned  $H_{kx} = H_{ky} = H_{kz} = 9,000$  A/m. The  $MFL_{\text{radial}}$  values are obtained at the underside of the dent over a 40mm x 40mm region, with the corresponding values from the 'no dent, no stress' case subtracted to eliminate the background effect. The data points obtained are appropriately mirrored to other quadrants yielding a final pattern as shown in Figure 27 (a). The corresponding experimental result for the 5mm deep axially-elongated dent is shown in Figure 5.27(b). The experimental sample was annealed so the  $MFL_{\text{radial}}$  result should primarily reflect the geometry contribution to the MFL signal. The results are in very good agreement – all peaks correspond although their positions are not identical. It is believed that the exact positions are dependent on the precise geometry of the dent rim. Although the main features of the dent rim were reproduced in the magnetic model geometry, sidewall slope and wall thickness were not exactly replicated.

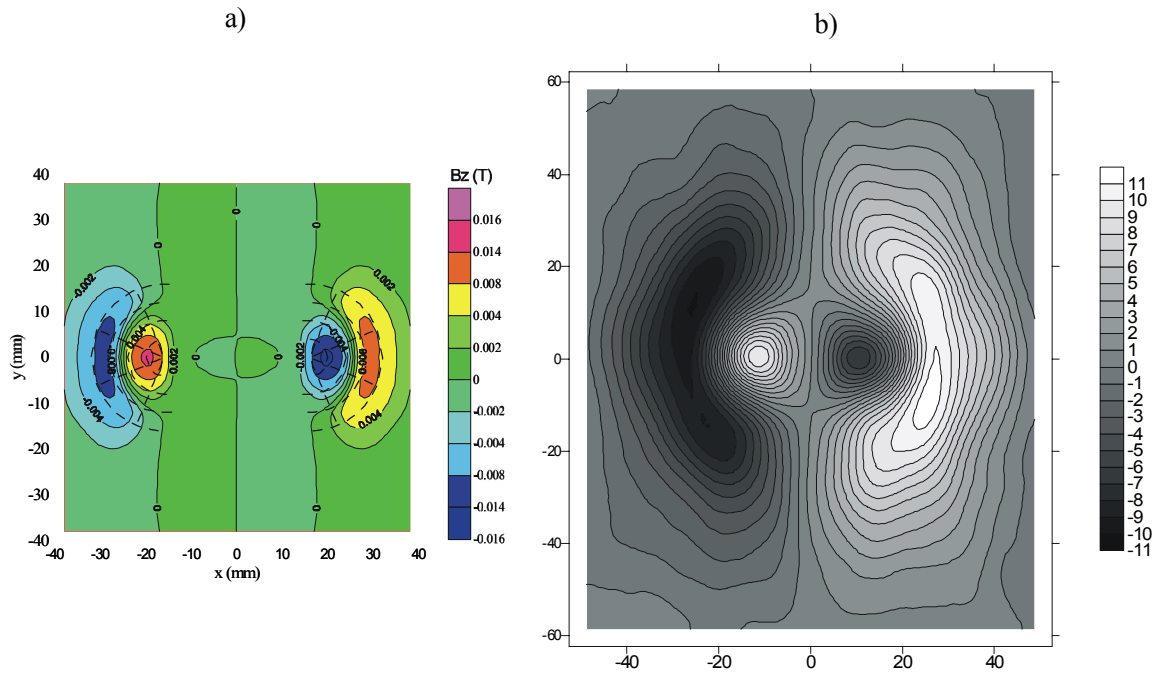


Figure 27. Comparison of modeled and experimental results for the “geometry only” evaluation of the 5-mm deep axially-oriented dent. a) The modeled  $MFL_{\text{radial}}$  signal contour map for the “geometry only” case. b) The experimental  $MFL_{\text{radial}}$  contour plot obtained from an annealed, 5mm deep axially-oriented dent. All of the main peak features are present, although the ability to model the precise dent geometry limits a prediction of the exact extent of each peak.

### 6.5.3 Axially Elongated Dent: Residual Stress Influences on the $MFL_{\text{radial}}$ Signal

The structural FEA results discussed in Section 5.3 were used for determining the level and direction of residual stresses around the dent that would affect the MFL pattern. As mentioned in Section 5.3, z-direction stresses were ignored because they were comparatively small. Additionally stresses in the applied field direction (in this case the axial or x-direction) were not included, since earlier studies showed that they have no effect on the MFL signal.

In the discussion that follows “upper half” refers to the top half-thickness of the dent (closest to the topside surface) whereas “lower-half” refers to the bottom-half thickness closest to the underside surface.

Figures 28 and 29 show the assignment of  $H_k$  values in individual upper half segments according to the stress FEA results seen in Section 5.3. The  $H_k$  values of modified segments are indicated in the figure caption. All other  $H_k$  values are assigned the “isotropic, no stress” value of 9000 A/m. There are also corresponding results for “lower-half” segments not shown here.

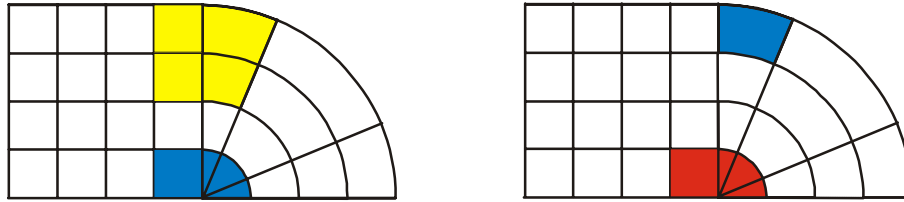


Figure 28. Assignment of  $H_k$  values for normal y stresses. (left) Dent segments in the upper half of the plate thickness (left) were assigned normal y stresses corresponding to  $H_k$  equal to 4,000 A/m (yellow), and 60,000 A/m (blue). (right) Dent segments in the lower half of the plate thickness were assigned the normal y stresses corresponding to  $H_k$  equal to 50,000 A/m (blue), and 2,000 A/m (red).

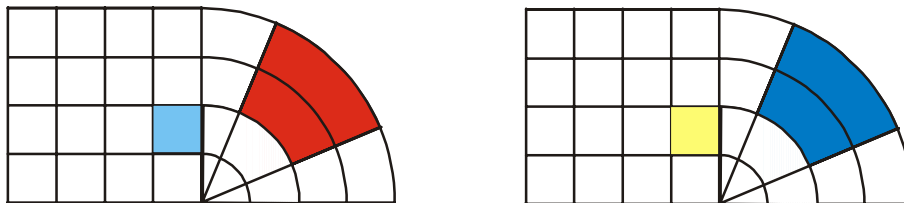


Figure 29. Assignment of  $H_k$  values for shear stresses. (left) Dent segments in the upper half of the plate thickness were assigned xy shear stresses corresponding to  $H_k$  equal to 6,000 A/m (red), and 20,000 A/m (blue). (right) Dent segments in the lower half of the plate thickness were assigned xy shear stresses corresponding to  $H_k$  equal to 30,000 A/m (blue), and 8,000 A/m (yellow).

### Circumferential (y) Stress Influences on the $MFL_{radial}$ signal

The advantage of modeling is the ability to turn ‘on’ or ‘off’ certain aspects of the model to examine their individual contributions to the MFL signal. In this case, stress regions can be turned on or off to evaluate their various contributions to the  $MFL_{radial}$  signal. Figures 30(a), (b) and (c) show the results of the dent base stresses incorporating the upper half, lower half, and combined stresses respectively for the circumferential (y) stresses applied as shown in Figures 28(a) and (b). Figures 30 (d), (e) and (f) show the effect of the dent rim stresses, incorporating the upper half, lower half, and combined stresses respectively. The combined effect of all normal circumferential stresses is shown in Figure 30(g).

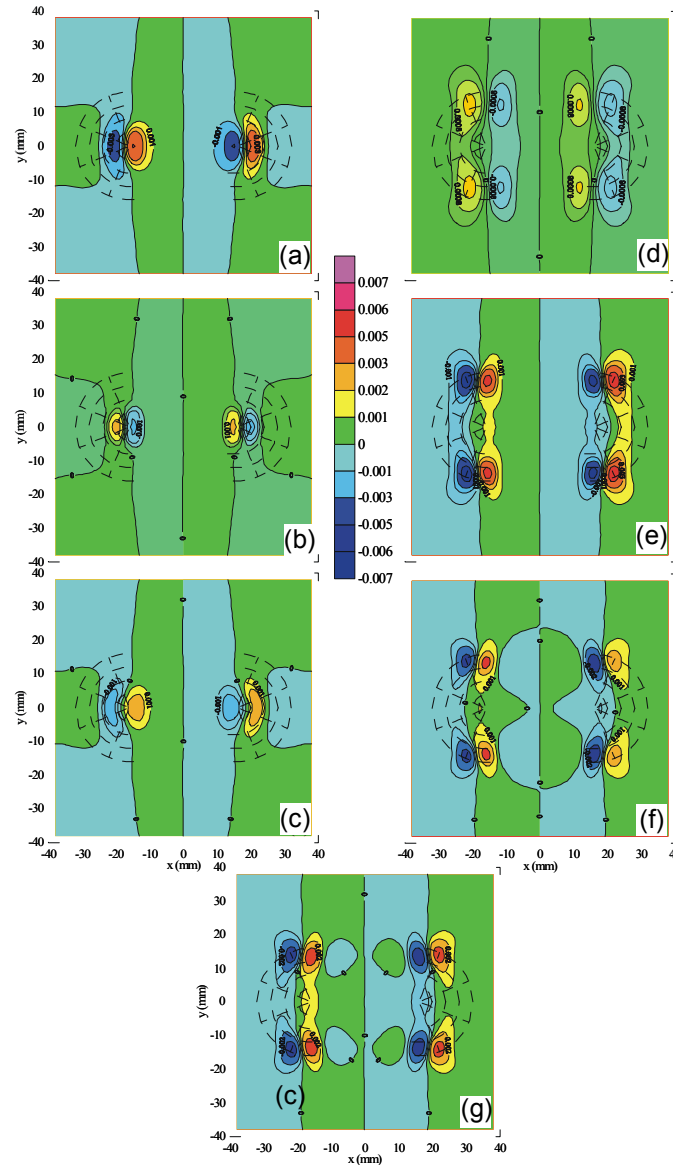


Figure 30. The contributions of normal residual circumferential (y) stresses on the  $MFL_{radial}$  signal. Figures (a), (b) and (c) show the base MFL stress patterns due to the upper half, lower half, and combined stresses respectively. Figures (d), (e) and (f) show

the corresponding outer rim stress patterns. The combined MFL pattern resulting from all y stresses is shown in (g).

### Shear (xy) Stress Influences on the $MFL_{\text{radial}}$ signal

A similar procedure to that shown for the circumferential stresses above was completed for evaluation of the shear stresses, but it is not included here for the sake of brevity. Figure 31 shows the effect of all shear stresses shown in Figure 29.

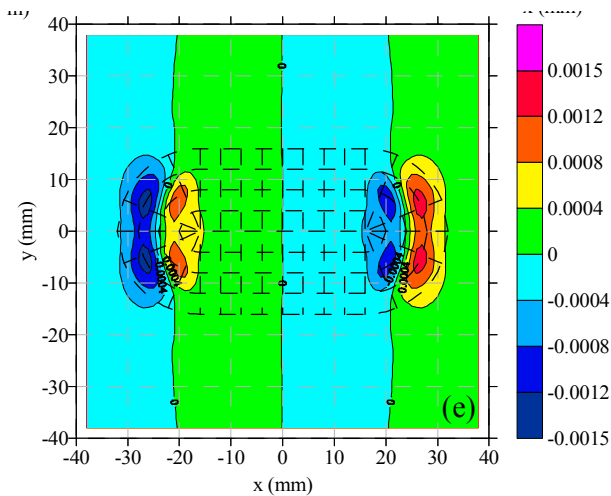


Figure 31. MFL pattern due to all the shear stresses shown in Fig. 29.

### Additional “Straight” Rim y Stress Regions: Influences on the $MFL_{\text{radial}}$ signal

A closer examination of the structural FEA stress patterns indicated that there were also normal circumferential (y) stresses along the sidewall of the dent; i.e. the ‘straight rim’ section. These were accounted for in the model as shown in Figure 32. The effect of the ‘straight rim’ stresses is shown in Figure 33.

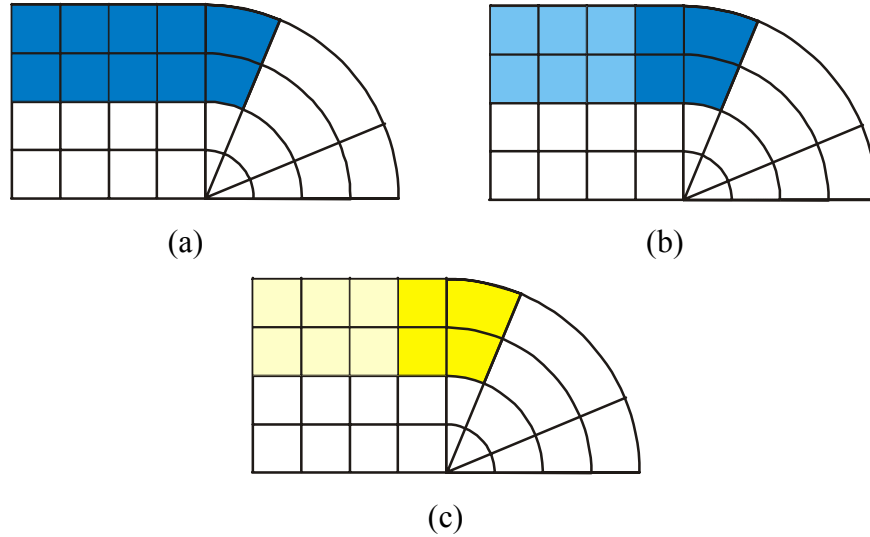


Figure 32. Quarter dent segments showing (a) lower half, high y-compressive stress region, (b) lower half, low y-compressive stress region (light blue) adjacent to a higher y-compressive stress region (dark blue), and (c) upper half, low y-tensile stress region (light yellow) adjacent to a high y-tensile stress region (dark yellow). The  $H_k$  values assigned to these regions are 50,000 A/m (dark blue), 30,000 A/m (light blue), 4,000 A/m (dark yellow), and 6,000 A/m (light yellow).

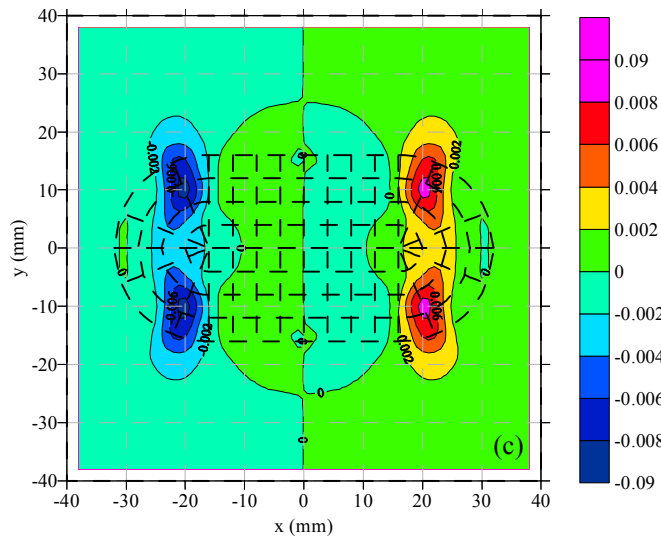


Figure 33. Effect on the  $MFL_{radial}$  signal of all of the 'straight rim' circumferential (y) stresses shown in Figure 32.

#### 6.5.4 Axially-Elongated Dent: Combined Effects of Stress + Geometry

Figure 34 shows the combined effect on the  $MFL_{radial}$  signal of all normal and shear stresses considered thus far. Figure 35 is the geometry-only signal which was

included earlier in this section and is reproduced again for easy comparison. Finally, Figure 36 shows the combined effects of all geometry and stresses on the signal. It is interesting to note the final diagram has a lower maximum scale value than the geometry-only case, indicating that the overall effect of the residual stress is to slightly lower some of the peaks. Furthermore, comparing Figures 35 and 36, the effect of stress causes the outer peak to extend in a “crescent” inwards towards the centre of the plot. This is because the large outer stress peaks seen in Figure 34 lie closer to the centre line of the dent than the large outer geometry peak, thus the combination appears to cause an extended crescent.

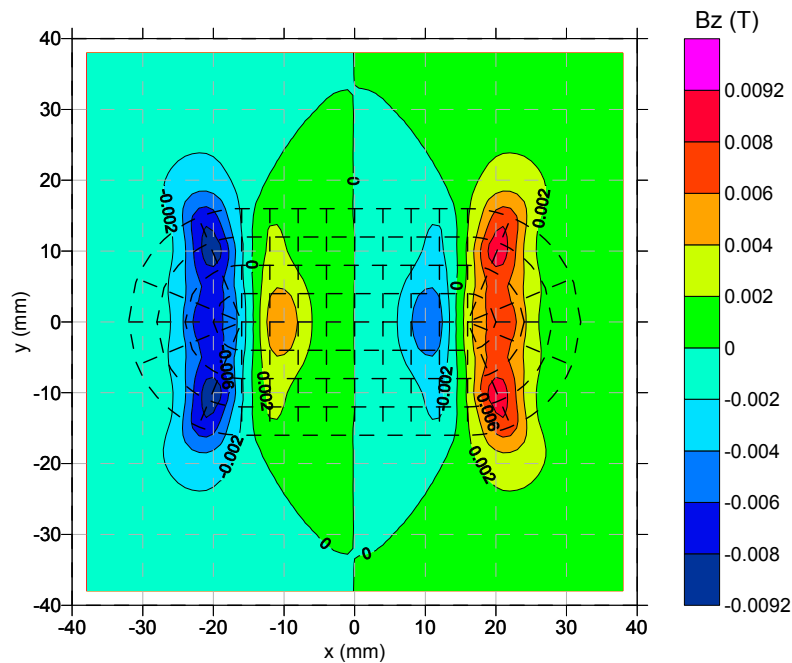


Figure 34. Combined effect of the normal circumferential (y) stresses (including straight and curved rim) and shear stresses on the  $MFL_{radial}$  pattern.

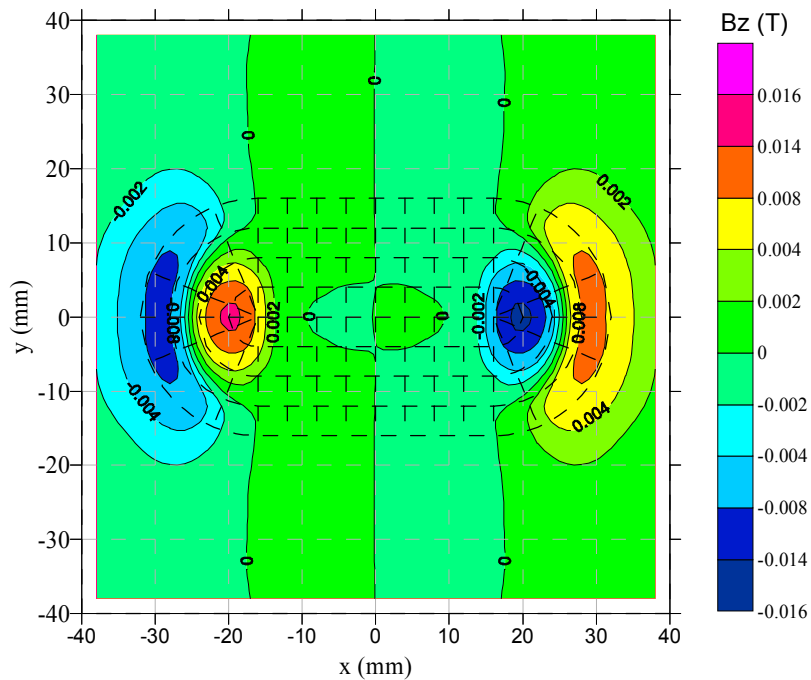


Figure 35. Geometry-only  $MFL_{\text{radial}}$  pattern shown earlier, reproduced here for ready comparison with Figures 34 and 36.



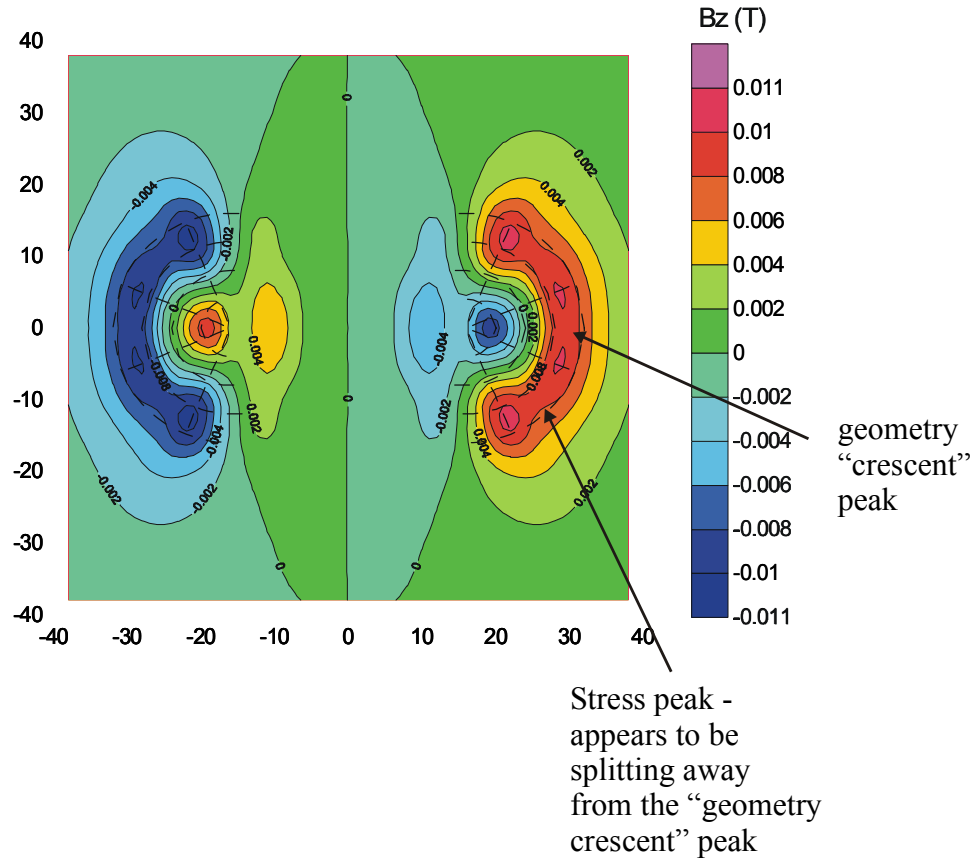


Figure 36. Final combined geometry + stress MFL<sub>radial</sub> pattern for the 5-mm deep, axially-elongated 2:1 dent.

### 6.5.5 Axially Elongated Dent: Comparison of Modeling and Experimental Results

Figure 37 displays the experimental MFL<sub>radial</sub> signal plot for the 5mm deep, axially-oriented 2:1 dent. This dent the same depth as the modeled dent, and the figure shows it in its unannealed state so it contains both residual stress and geometry peaks. In comparing it with the modeled result in Figure 36 the agreement is qualitatively very good for all of the main peaks, which are all reproduced in the model result. The differences in the shapes of the peaks is to be expected since the model geometry capability is not sufficiently sophisticated to reproduce all of the subtle geometry features of the dent such as exact sidewall slope.

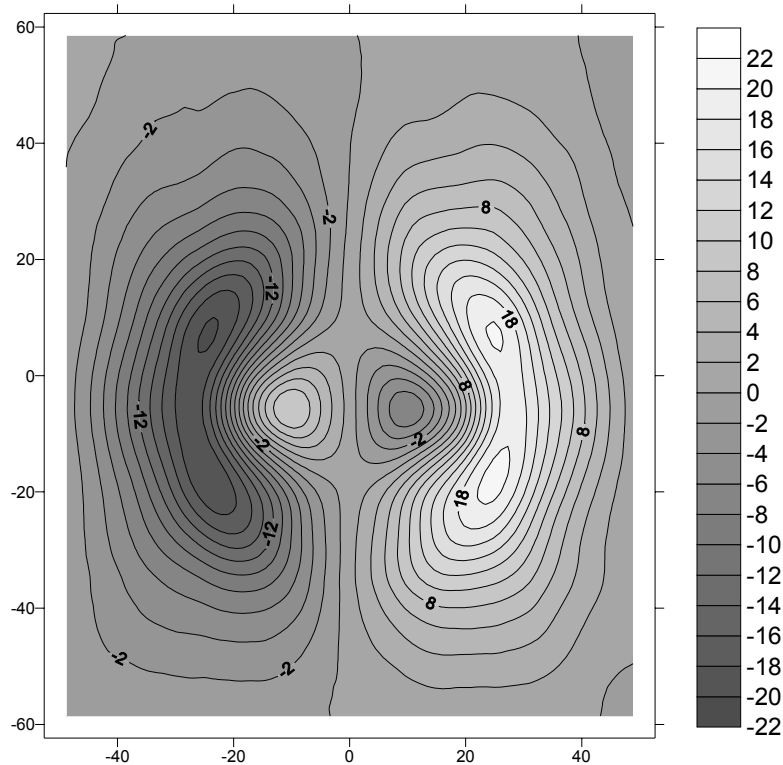


Figure 37. Experimental  $MFL_{radial}$  smoothed contour plot for an axially-elongated 2:1 dent of 5-mm depth (unannealed). This can be compared directly to the modeled result shown in Figure 36.

As noted earlier, axial dents of higher aspect ratio were also investigated as part of an extended study. Interestingly, it was found that as the high aspect ratio dents increased in depth, the stress ‘halo’ actually split off and “moved” towards the centre of the plot. Figure 38 (a) shows the experimental  $MFL_{radial}$  result for a 4:1 axially-oriented dent of depth 5mm, and Figure 38 (b) shows the same for a 6mm deep dent. These two experimental plots suggest that as the dent deepens the stress peak moves increasingly to the middle of the plot, appearing to ‘split off’ from the geometry crescent. This was not observed significantly in the experimental 2:1 case since the effect becomes more pronounced as the dent elongates and the geometry peaks move away from the central sidewall peaks. It is believed that the modeling data (Figure 36) supports this observation, since as the dent aspect ratio increases, the geometry peak will continue outwards but the stress peak (which is influenced heavily by the straight rim stresses) will not.

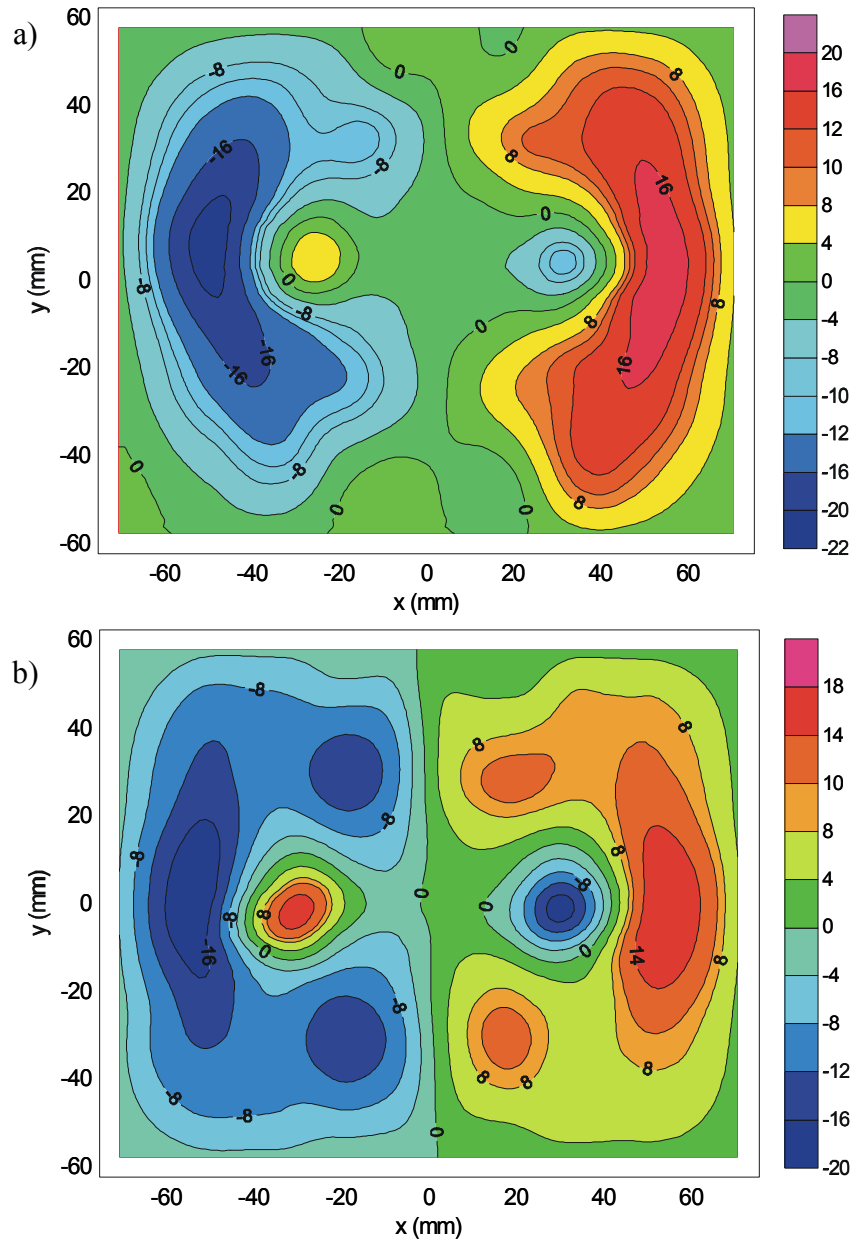


Figure 38. Experimental  $MFL_{radial}$  contour plot from a 4:1 axially-oriented dent of a) 5mm depth and b) 6mm depth.

## 6.6 Magnetic FEA Modeling Results: Circumferentially Elongated Dents

In this case the model is identical to that pictured in Figure 25, except that the long axis of the dent is oriented parallel to the magnet rather than perpendicular to it as shown. Note that the background is the same as that used for the axially-oriented dent case considered in Section 6.5.1.

### 6.6.1 Circumferentially-Elongated Dent: Geometry Only Case

As in the axially-oriented geometry-only model discussed in Section 5.5.2, this case considers only the geometry contribution to the signal. Therefore all of the segments in the dent are considered to have zero stress, and are assigned  $H_{kx} = H_{ky} = H_{kz} = 9,000$  A/m. The  $MFL_{\text{radial}}$  values are obtained at the underside of the dent over a 40mm x 40mm region, with the corresponding values from the 'no dent, no stress' case subtracted off to eliminate the background effect. The data points thus obtained are appropriately mirrored to other quadrants yielding a final pattern as shown in Figure 39(a). The corresponding experimental result (annealed) for the 5mm deep circumferentially-elongated dent is shown in Figure 39(b). The experimental sample was annealed so the  $MFL_{\text{radial}}$  result shown primarily reflects the geometry contribution to the MFL signal. Overall the patterns are similar, however the extent of the inner central peaks is somewhat smaller in the experimental result than in the modeled pattern, and again it is believed that this is attributed to a dependence of the peak shape on the detailed geometry of the dent rim, which was not reproduced exactly in the model. Further work will assist us to clarify the differences.

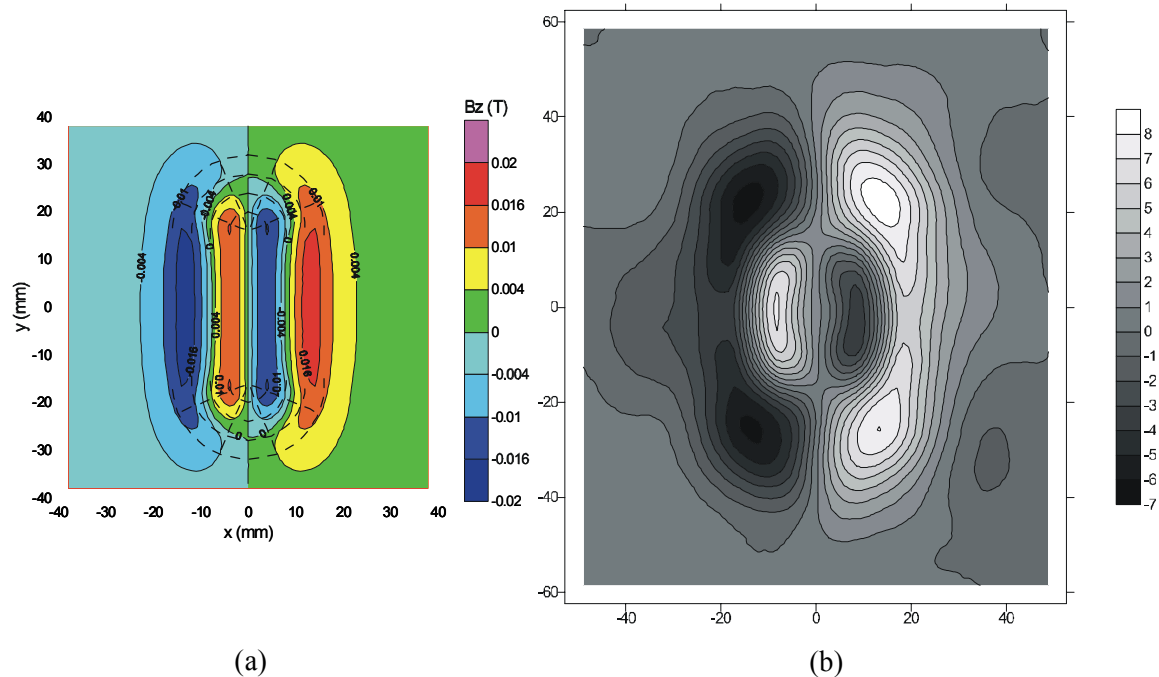


Figure 39. Comparison of modeled and experimental results for the “geometry only” evaluation of the 5-mm deep circumferentially-oriented dent. a) The modeled MFL<sub>radial</sub> signal contour map for the “geometry only” case. b) The experimental MFL<sub>radial</sub> contour plot obtained from an annealed, 5mm deep circumferentially-oriented dent.

### 6.6.2 Circumferentially-Elongated Dent: Stress Influences on the $MFL_{\text{radial}}$ Signal

The structural FEA results discussed in Section 5.3 were used for determining the level and direction of stresses around the dent that would affect the MFL pattern. Note that even though the same structural FEA results can be used, in the magnetic FEA model

the defect is now rotated  $90^\circ$  compared to the axially-elongated case. Therefore the x and y directions in the structural model are now effectively reversed. As mentioned in Section 5.5, radial stresses were ignored because they were comparatively small. Additionally stresses in the axial (magnetization) direction were not included, since, as mentioned earlier, they have no effect on the MFL signal.

The separate effects of turning stress ‘on’ and ‘off’ in different regions of the rim were outlined in the Section 5.5.3 discussion of the axially-elongated dent. The same procedure was conducted for the circumferentially-elongated dent, however only the final modeled result is included here for brevity. Figure 40 shows the final stress-generated  $MFL_{\text{radial}}$  contour plot, including the effects of all normal circumferential and shear stresses. The ‘straight rim’ stresses that were important in the axially-oriented dent case do not contribute here because they lie in the applied field direction and therefore do not affect the MFL signal.

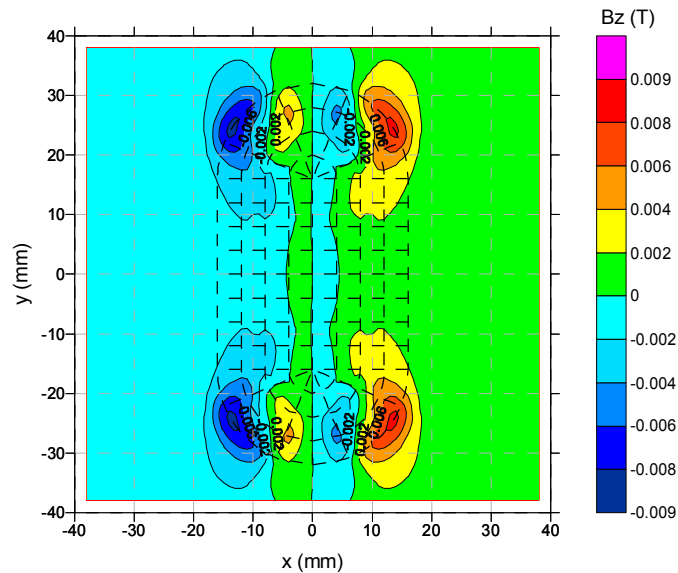


Figure 40. Effect on the  $MFL_{\text{radial}}$  signal of all of relevant stresses in and around the circumferentially-oriented, 2:1 5 mm deep dent.

### 6.6.3 Circumferentially-Elongated Dent: Combined Effects of Stress + Geometry

Figure 41 shows the combined effects of stress and geometry for the circumferentially-elongated dent. First it is worthwhile to note that the stress effects in this case are relatively small, as suggested by comparing the MFL scale on this diagram with that of Figure 40. (This was not the case for stresses in axially-oriented dents, where the stress MFL signal was only slightly smaller than the geometry signal). Furthermore, as seen in Figure 40, the stress effects are primarily located at the extreme ends of the dent, and this is reflected in slight peaks produced at the end of the main geometry peaks of Figure 41.

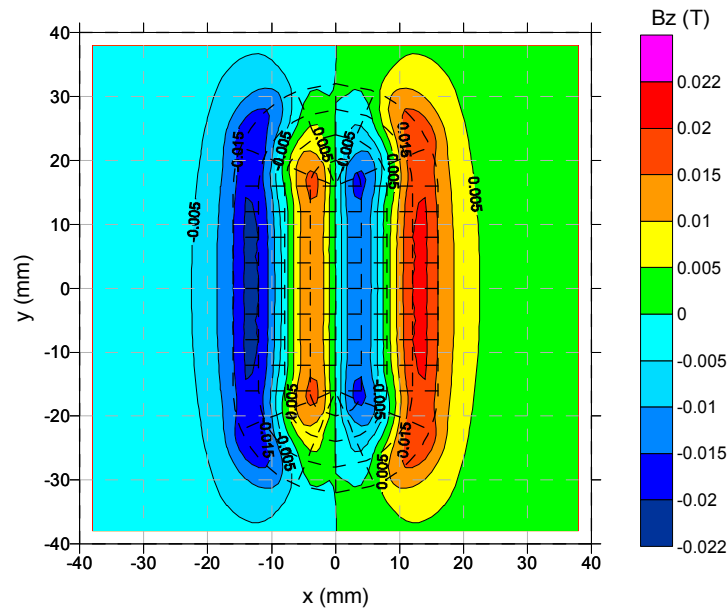


Figure 41. Final combined geometry + stress  $MFL_{radial}$  pattern for the 5-mm deep, circumferentially-elongated 2:1 dent.

#### 6.6.4 Circumferentially-Elongated Dent: Comparison of Modeling and Experimental Results

Figure 42 shows the experimental data  $MFL_{radial}$  signal plot for the 5mm deep, circumferentially-elongated 2:1 dent (scaled to match the modeled result). This dent is approximately the same size as the modeled dent, and the figure shows it in its unannealed state so it contains both stress and geometry peaks. In comparing it with the modeled result in Figure 41 the agreement is qualitatively very good - all of the main peaks in the experimental plot are reproduced in the model result. Since most of the stress peaks correspond with the ‘ends’ of the geometry peaks it is somewhat difficult to differentiate the specific stress contribution to the result – particularly since in this case the stress effects tend to be somewhat less significant than in the axially-elongated dent case.

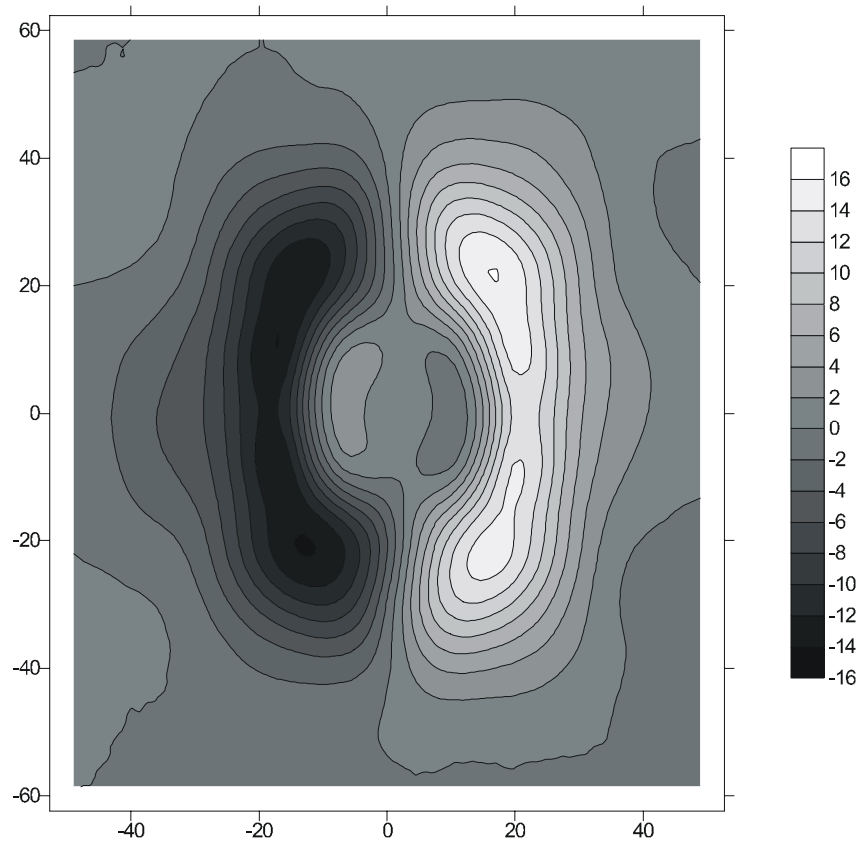


Figure 42: Experimental MFLradial contour plot for a circumferentially-elongated dent of depth 5 mm (unannealed). This can be compared directly to the modeled result shown in Figure 41.

## 6.7 Circular Dents with Included Corrosion Pits:-Experimental and Modeling Results

### 6.7.1 Experimental Results:-Circular Dent + Corrosion Pit

In this section the effects of introducing a small corrosion pit into a circular dent are considered. As in earlier denting experiments, plate thickness was 3mm. Three different cases were examined experimentally:

1. A 3mm diameter, through-wall pit, introduced into an undented plate
2. A 'blind' (not through wall) 3mm diameter, 2mm deep pit introduced into the centre of a 3mm deep circular dent of approximate diameter equal to 40mm (recall that the sample plate is 3mm thick); and
3. A 3mm diameter through-wall pit introduced into the centre of a 5mm deep circular dent of approximate diameter equal to 40mm.

All pits were electrochemically milled into the sample to simulate the true corrosion pitting processes. The blind pit was introduced from the underside of the sample. Although MFL measurements were made on both the topside and underside of the plate, only the underside results are presented here.

Figure 43 (a), (b) and (c) show the experimentally measured  $MFL_{\text{radial}}$  component signal for the three cases in the order corresponding to that listed above. The corrosion pit signal and the dent signals superimpose, and in this case, the features of each can be clearly seen, (although the 'blind' pit signal case in Figure 43(b) is somewhat less obvious than in the other two cases).

Figures 44 (a,) (b) and (c) show the same series of experimental results except for the  $MFL_{\text{axial}}$  case. In this case the corrosion pit signal appears as a 'double bump' region in the centre of the dent signal. (Compare Figure 44(c) for example with Figure 14 which has no pit). However in general, the pit signal is less obvious than it is for the  $MFL_{\text{radial}}$  case shown in Figure 43.

Finally, Figure 45(a,) (b) and (c) show the same series of experimental results except for the  $MFL_{\text{circ}}$  case. In this case the corrosion pit signal is very small even in the 'no dent' case and essentially negligible when a dent is present.



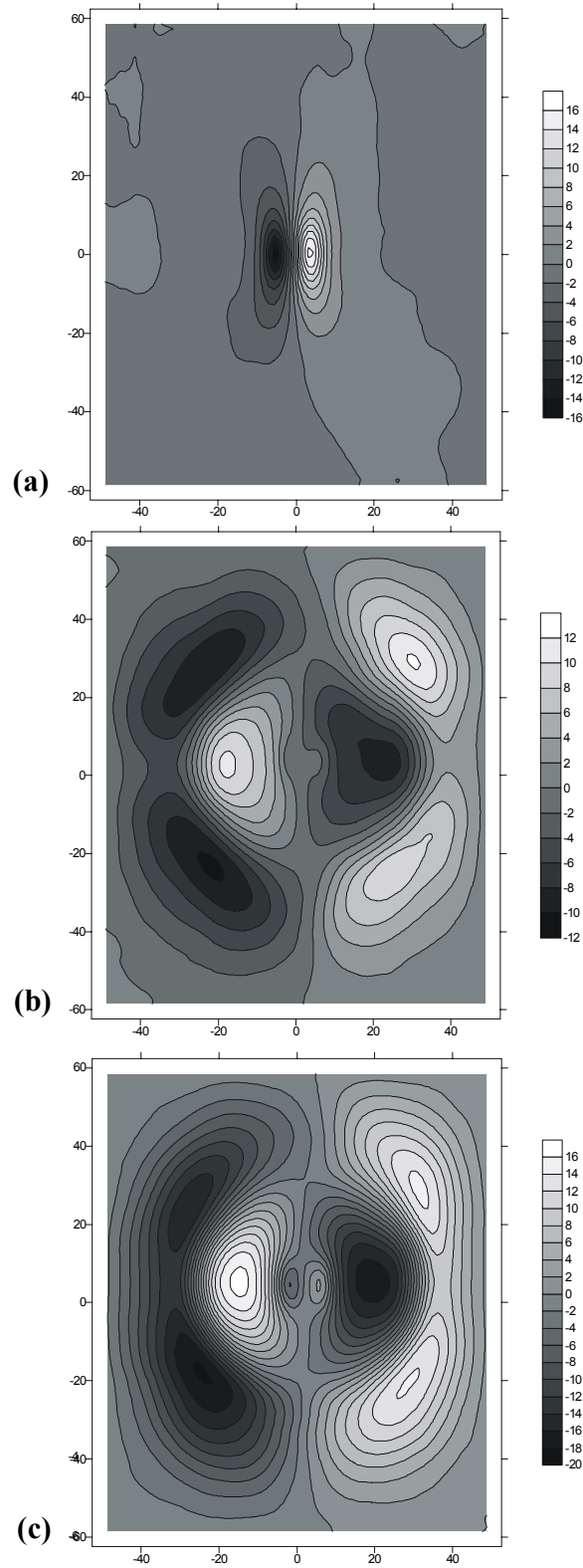


Figure 43. Underside MFL<sub>radial</sub> plots for (a) a 3mm diameter through-wall corrosion pit in an undented plate, (b) a 3mm diameter blind pit in a 3mm deep circular dent, and (c) a 3mm diameter through-wall pit in a 5mm diameter deep circular dent.

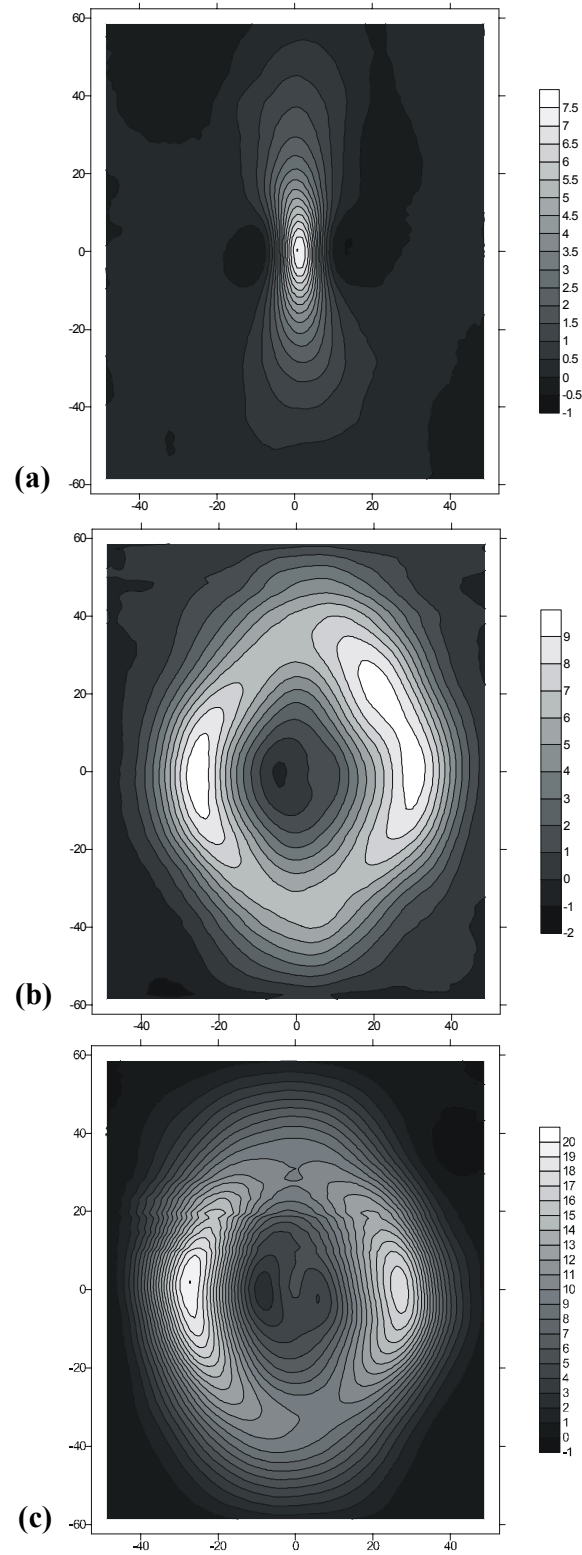


Figure 44. Underside MFL<sub>axial</sub> plots for (a) a 3mm diameter through-wall corrosion pit in an undented plate, (b) a 3mm diameter blind pit in a 3mm deep circular dent, and (c) a 3mm diameter through-wall pit in a 5mm deep circular dent.

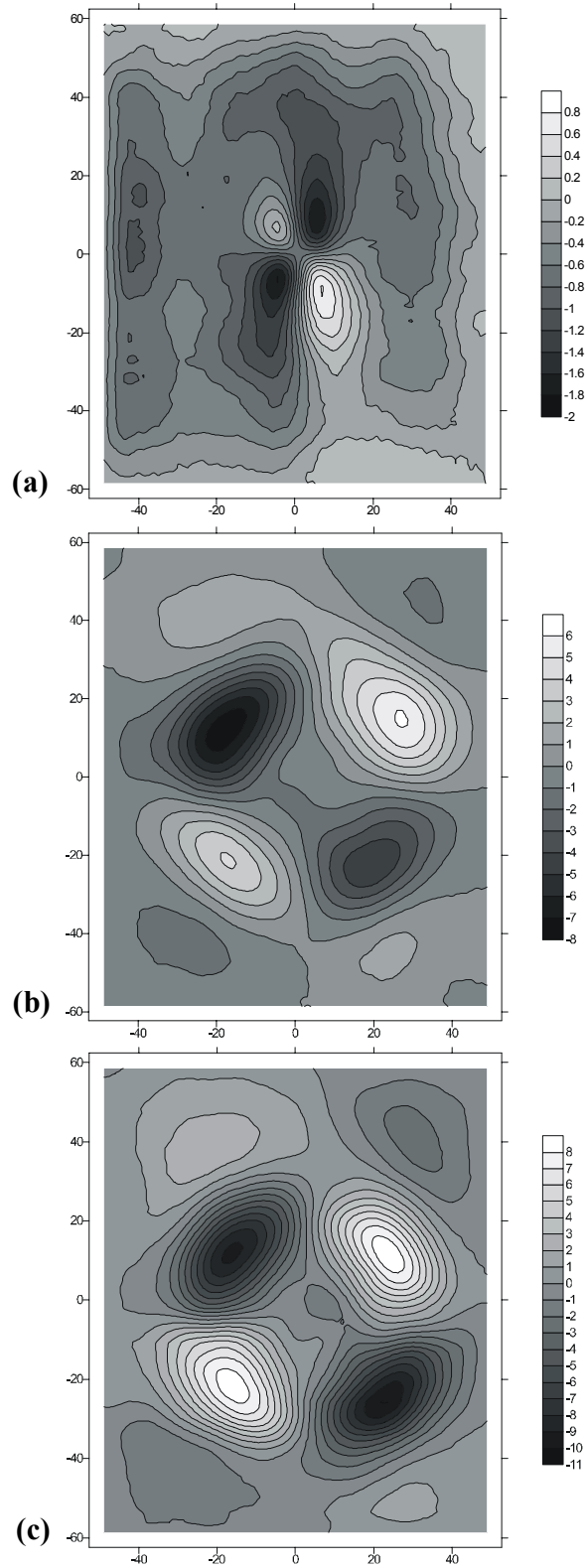


Figure 45. Underside MFL<sub>circ</sub> plots for (a) a 3mm diameter through-wall corrosion pit in an undented plate, (b) a 3mm diameter blind pit in a 3mm deep circular dent, and (c) a 3mm diameter through-wall pit in a 5mm circular dent.

### 6.7.2 Magnetic FEA Modeling Results: Circular Dent + Corrosion Pit

Dents containing corrosion pits were modeled for slightly different geometries than for the experimental measurements, however, only qualitative comparisons are expected at this stage and the results are readily comparable. In the magnetic FEA model, the pit radius was 3 mm and the sample plate 4-mm thick. The pits were through-wall. The modeled circular dents had a base radius of 12 mm and an outer radius of 28 mm. The dent depth was 8 mm. Finally, stresses were not modeled for these cases.

Figure 46 (a) and (b) shows the case for two dents—the first with no pit and the second containing a central corrosion pit as described above. The additional peaks associated with the pit can be seen clearly in Figure 45(b), as in the experimental  $MFL_{\text{radial}}$  component peaks in Figure 43.

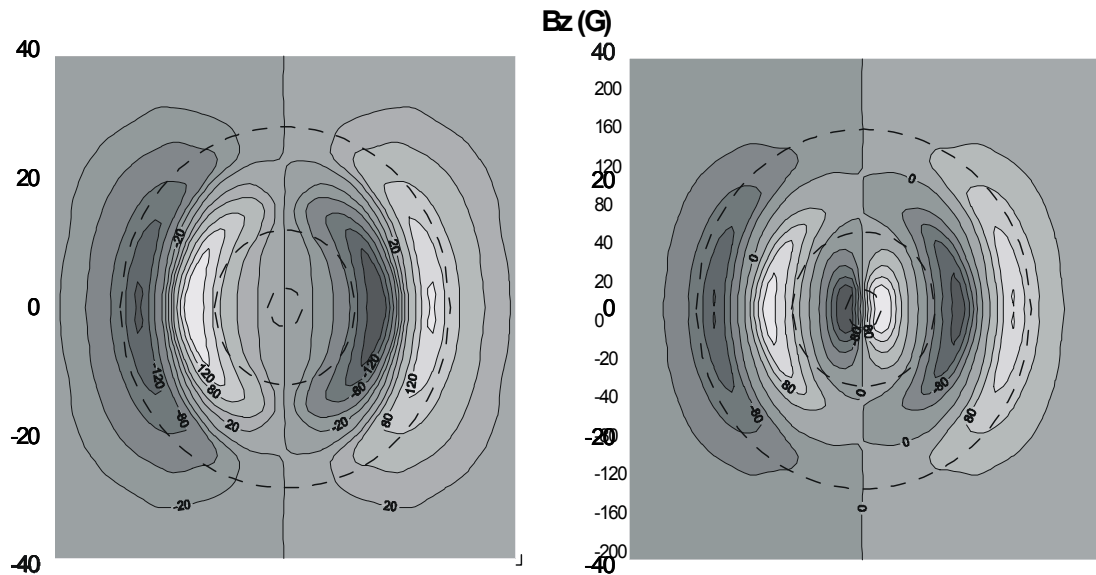
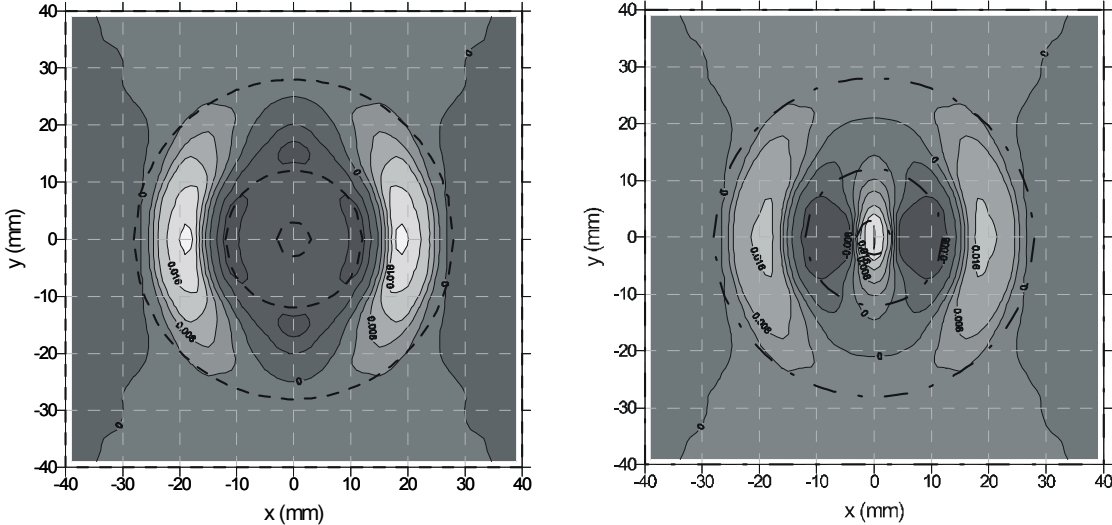


Figure 46. Magnetic FEA  $MFL_{\text{radial}}$  model results for circular dent + corrosion defect. (a) Circular dent-only modeled  $MFL_{\text{radial}}$  component. (b) Circular dent with included corrosion pit modeled  $MFL_{\text{radial}}$  component.

Figure 46 shows a similar result, but for the  $MFL_{\text{axial}}$  component signal. In this case the modeled pit signal is more obvious than the experimental results shown in Figure 44. This is because the detector is necessarily further away from the surface in the experimental axial component case (compared with the radial component orientation) and the signal is correspondingly weaker.



(a) Circular dent-only modeled  $\text{MFL}_{\text{axial}}$  component. (b) Circular dent with included corrosion pit, modeled  $\text{MFL}_{\text{axial}}$  component.

Finally, on observation of Figure 47(b) it is clear that the  $MFL_{axial}$  corrosion pit peaks are of opposite polarity to the adjacent central dent geometry peaks. One would expect that as the corrosion pit ‘grows’ relative to the dent that the peaks will overlap and even partially cancel one another. This is indeed the case. Figure 48 shows this result for three different corrosion pit diameters of 2mm, 4mm and 24mm. The corrosion pit signal grows with respect to the dent signal and overlap occurs at 24mm.

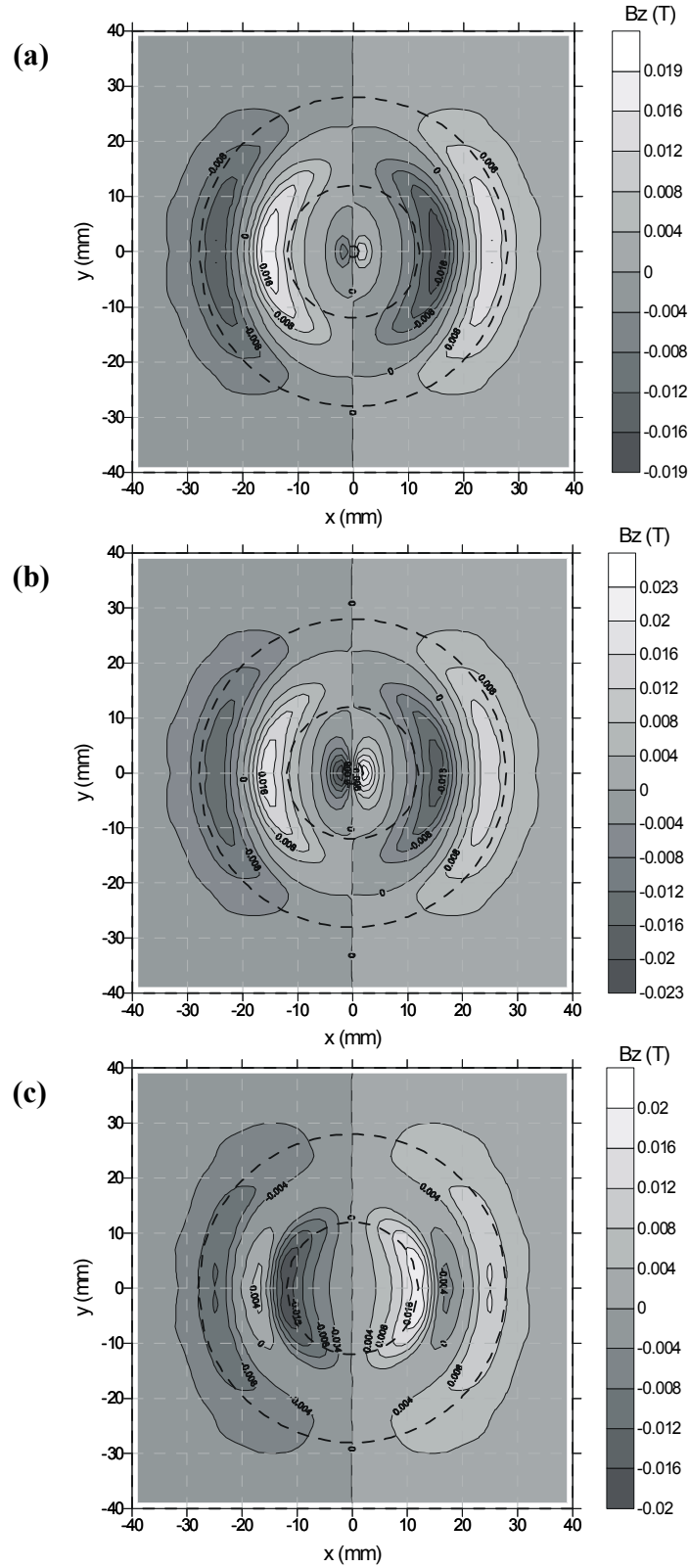


Figure 48. Underside MFL radial component, corrosion pit + circular dent. (a) Corrosion pit diameter = 2mm, (b) Corrosion pit diameter = 4mm, (c) Corrosion pit diameter = 24mm.

## 6.8 Web-Based Database of MFL Signals from Dented Samples

It should be clear to the reader at this point that, although this report has included a large number of plots and results, there are an even greater number that were not shown. As outlined at the beginning of Section 5.2, for example, a total of 120 individual MFL scans were produced experimentally in the main part of this work on 2:1 aspect ratio dents. A parallel experimental study on 4:1 dents produced a similar number of plots, with still more plots associated with the corrosion pit work. The modeling resulted in a comparable amount of data. In total approximately 400 data plots were produced as part of Phase I of this MFL and mechanical damage study. To effectively document this information for future use by others a web-based 'template library' that catalogues the results is proposed. The library will be made available for use by other interested parties to assist the transfer of project results to industry. In the fourth quarter of 2006, work to develop the design and construct the proposed template library will be initiated.

Figure 49 shows an example of the 'entry window' for the proposed database of experimental MFL signals. The dent Aspect Ratios are given in the left column where 1:1 is the circular dent, 2:1 and 4:1 represent axially-elongated dents and 1:2 and 1:4 represent circumferentially-elongated dents. The three table columns indicate MFL radial, axial and circumferential component signals measured from topside and underside. When the database is online, clicking on a particular link will take the user to a .pdf page containing both unannealed and annealed data plots of increasing dent depths from 3mm to 7mm, resulting in a total of 10 plots for each link. Greater functionality can be added as the project progresses, but it is believed that this database will provide excellent accessibility for interested users to gain easy access to the results of this study.

	<b>Topside Underside</b>	<b>Topside Underside</b>	<b>Topside Underside</b>
<b>Aspect Ratio</b>	<b>Radial</b>	<b>Axial</b>	<b>Circumferential</b>
<b>1:1 large</b>	<a href="#">1:1lgTR</a>    <a href="#">1:1lgUR</a>	<a href="#">1:1lgTA</a>    <a href="#">1:1lgUA</a>	<a href="#">1:1lgTC</a>    <a href="#">1:1lgUC</a>
<b>2:1 normal</b>	<a href="#">2:1TR</a>    <a href="#">2:1UR</a>	<a href="#">2:1TA</a>    <a href="#">2:1UA</a>	<a href="#">2:1TC</a>    <a href="#">2:1UC</a>
<b>4:1 normal</b>	<a href="#">4:1TR</a>    <a href="#">4:1UR</a>	<a href="#">4:1TA</a>    <a href="#">4:1UA</a>	<a href="#">4:1TC</a>    <a href="#">4:1UC</a>
<b>1:2 normal</b>	<a href="#">1:2TR</a>    <a href="#">1:2UR</a>	<a href="#">1:2TA</a>    <a href="#">1:2UA</a>	<a href="#">1:2TC</a>    <a href="#">1:2UC</a>
<b>1:4 normal</b>	<a href="#">1:4TR</a>    <a href="#">1:4UR</a>	<a href="#">1:4TA</a>    <a href="#">1:4UA</a>	<a href="#">1:4TC</a>    <a href="#">1:4UC</a>

Figure 49. Database of MFL results for dented samples - topside and underside.

## 7. Conclusions

Work in the current year has been extremely successful – with the magnetic models helping to interpret many details and features of MFL signals that will prove to be extremely important in establishing dent severity. Qualitative agreement between models and experimental results has been excellent. Furthermore, all work is on-time and on-budget. A summary of specific results and details of this year's study is provided below.

### 1. Experimental comparison of $MFL_{radial}$ , $MFL_{axial}$ and $MFL_{circ}$ dent signals

Experimental studies examined both topside and also underside MFL signals from a range of depths, both in the axial and circumferential orientation. The following points were noted:

- The  $MFL_{radial}$  signal component consistently displays the largest and most detailed signals. This is due to the fact that the sensor lies closer to the surface in this orientation than in the other two.
- The  $MFL_{radial}$  and  $MFL_{circ}$  signals contain distinct stress-related and also geometry-related features (peaks). In general the central peaks tend to be geometry related, with dent rim stresses reflected in shoulder peaks. The  $MFL_{axial}$  component appears to have no specific stress-related features and also appears similar to signals produced by corrosion pits.
- All MFL signal features diminish slightly with stress-relief annealing, however the magnitude of the shoulder peaks is considerably affected by annealing, reinforcing the conclusion that they tend to be related to residual stress.

A major conclusion from this aspect of the work is that, for dent detection and sizing, inspection tools should measure all three components of the MFL signal, rather than just the  $MFL_{axial}$  signal as is typical in most cases.

### 2. Axially-elongated 2:1 aspect ratio dents: modeling and experimental studies

Both geometry and stress have considerable and interesting effects on the axially elongated dent signals:

- The geometry signal displays a characteristic '4 peak'  $MFL_{radial}$  signature along the line of the dent in the applied field direction. The two outside peaks are associated with the outer dent rim 'corner', while the two inner peaks originate from the corner at the dent base. This result is similar to that seen in circular dents – however as the dent aspect ratio increases the peaks migrate further away from the dent centre.
- The main stress contribution to the  $MFL_{radial}$  signal is associated with the dent rim 'sidewall' – i.e. the rim along the long side of the dent. This produces a significant vertical peak which tends to be positioned approximately over the central dent geometry peak.
- The combined effect of stress+geometry on  $MFL_{radial}$  signals is very interesting in this case, since the dent sidewall stress contribution lies over the inner dent geometry peak but is of opposite polarity. This has two effects –
  1. to diminish the size of the inner geometry peak
  2. to 'create' an apparent additional peak in the centre dent sidewall rim region. This peak is actually a composite of geometry+stress effects.



This is particularly notable because accurate interpretation of this signal would likely have been impossible without the contribution from the modeling study.

### **3. Circumferentially-elongated 2:1 aspect ratio dents: modeling and experimental studies**

The results of experimental and modeling studies for the  $MFL_{\text{radial}}$  signals for circumferentially-oriented elongated dents are summarized below:

- The geometry signal comprise 4 peaks as with the earlier circular and axial dent cases, however due to the circumferential elongation of the dent these central peaks are much closer together and also elongated.
- Sidewall dent rim stresses have little effect on the MFL signal in this orientation. The stress effects on the signal are mainly in the form of shoulder peaks at the extreme ends of the signal (in the circumferential direction).
- Combined stress + geometry signals are relatively simple to interpret in this case and represent a straightforward superposition of the two effects on the signal.

### **4. Circular dents containing corrosion pits: modeling and experimental studies**

This aspect of the current year study was undertaken to examine the combined MFL signals from pits located within circular dents. Through-wall pits of 2, 4 and 24mm were created in 40mm diameter circular dents. Both modeling and experimental work indicated that the MFL signals for the combined pit+dent were a simple superposition of the two signals. The pit was centered in the middle of the dent, so clear signals from pit and dent were seen when the dent was relatively small. In the 24mm diameter pit there was considerable overlap with signals and interpretation became more difficult.

### **5. Web-based database – preliminary work**

The ultimate goal of this project is to be able to have MFL signal results from dents of known shapes and stresses. With a very large number of results, effective presentation becomes an issue. We present a relatively simple proposed format for a web-based, results spreadsheet which should allow for easy access to both modeled and experimental results of this study. Further development of this database will proceed as the project evolves.

## 8. References

- [1] D.L. Atherton. (Oct. 1986) "Effect of line pressure on the performance of magnetic inspection tools for pipelines, Oil and Gas J., V84, No.43, 86-89.
- [2] Gas Research Institute contract #5093-260-2605 "3D details of Defect-Induced MFL and Stress in Pipelines", Annual Reports 1998-2002.
- [3] L. Clapham and D.L. Atherton, 2003, "Stress effects on MFL signals", Pipeline and Gas Technology, Hart Publications, Texas, June 2003, 20-27, also [www.PipeLineandGasTechnology.com](http://www.PipeLineandGasTechnology.com).
- [4] L. Clapham, A. Plotnikov and D.L. Atherton, "Local Stress Effects on MFL Steels", 2000 International Pipeline Conference, October 1-5, 2000, Calgary, Canada.
- [5] DOT final report DTRS56-96-C-0010, Bubenik and Nestleroth (Battelle) "In-Line Inspection Technologies for Mechanical Damage and SCC in Pipelines, June 2000.
- [6] DOT contract DTRS56-02-T-0002, Nestleroth (Battelle/PRCI) "Mechanical Damage Inspection using MFL Technology", 2002-04.
- [7] DOT contract DTRS56-00-H-0004, Morrissey(GTI/Battelle)"Better Understanding of Mechanical Damage in Pipelines", 2000-02.
- [8] Infolytica Corp. P.O. Box 1144, 300 Leo Pariseau, Suite 2222, Montreal, Quebec. H2W 2P4, Canada. [www.infolytica.com/en/](http://www.infolytica.com/en/).
- [9] Gas Technology Institute contract # PR-GRI-8682 "3D Details of Defect-Induced MFL and Stress in Pipelines (Detection of Mechanical Damage using Magnetic Flux Leakage). Annual Report, 2004
- [10] Surfer 7, Golden Software, Inc., 809 14<sup>th</sup> St., Golden, Colorado, 80401, USA. [www.goldensoftware.com](http://www.goldensoftware.com)
- [11] C.-G. Stefanita, D. L. Atherton and L. Clapham, "Plastic versus elastic deformation effects on magnetic Barkhausen noise in steel," Acta Mater., vol. 48, pp. 3545-3551, 2000.
- [12] ANSYS Canada Ltd. 54 Parkside Drive, Waterloo, Ontario, N2L 5Z4 Canada, [www.ansys.com](http://www.ansys.com)
- [13] The MathWorks Inc., 3 Apple Hill Drive Natick, MA 01760-2098, USA. <http://www.mathworks.com/>